

Quantum Telecloning

Diplomarbeit an der Fakultät für Physik
der
Ludwig-Maximilians-Universität München
Arbeitsgruppe Prof. Dr. Harald Weinfurter

Julia Lau

16. Februar 2004

Erstgutachter: Prof. Dr. Harald Weinfurter
Zweitgutachter: Prof. Dr. Hans J. Briegel

Contents

1	Introduction	3
2	Theory	5
2.1	Polarised light	5
2.2	Qubits	6
2.3	Entanglement	7
2.4	Quantum teleportation	8
2.5	Quantum cloning	10
2.5.1	No-cloning theorem	10
2.5.2	Optimal quantum cloning	11
2.5.3	The 'classical' limit	12
2.6	Quantum telecloning	13
3	Implementation	19
3.1	Parametric down conversion	19
3.2	Bell state analysis	22
3.2.1	Influences of beam splitter parameters on the Bell state analysis . .	24
3.2.2	Hong Ou Mandel dip	28
3.3	Measurement of density matrices	32
4	Experiment	35
4.1	The setup	35
4.1.1	The source of entangled photons	36
4.1.2	Weak coherent state preparation	42
4.1.3	The analysers	43
4.2	The overlap	45
4.2.1	Classical interference	45
4.2.2	Interference between two down conversion photons	46
4.2.3	Interference between a down conversion photon and a weak coherent state	49
4.3	Quantum teleportation	53
4.4	Quantum telecloning	55
4.4.1	Telecloning of three different input states	56

CONTENTS

4.4.2	Measurement of the density matrices of the clones	59
5	Summary	63
A	Appendix	65
A.1	Determination of beam splitter parameters	65
A.2	Representations of photon states	67

1 Introduction

Quantum mechanics offers new possibilities of information processing and communication. About 20 years ago this initiated the field of quantum information, which is based on the idea of using quantum systems as carriers of information. The fundamental difference to classical information is that quantum systems can exist in superposition states.

Well known examples for possible applications of quantum information theory are quantum computers that could dramatically speed up the solution of certain mathematical problems like factoring by simultaneously processing information encoded in superpositions of states, or quantum cryptography which makes truly secure communication possible for the first time and relies on the reduction postulate.

Most quantum computation and communication schemes are based on entanglement between two or more particles where the information is encoded in the correlations between particles rather than in the single particles. Entanglement can connect any two points in space-time in such a way that a measurement on one particle instantaneously influences the state of another particle, which can be arbitrarily far away. But all quantum communication schemes additionally require the transmission of classical information which cannot proceed faster than light, in this way causality is preserved. An impressive illustration of this feature is given by the scheme of quantum teleportation [3], where a quantum state is transferred between two quantum systems.

In contrast to classical information quantum information cannot be copied with arbitrary precision [10], there exists an upper bound for the quality of copies of quantum states which is achieved by a process called optimal quantum cloning [2, 5, 12].

Though quantum information theory advanced very fast, the progress in the experimental realisation of the proposals was comparably slow, mainly due to the lack of an efficient source of entangled particles. Type II spontaneous parametric down conversion turned out to be a bright and stable source of polarisation entangled photon pairs [7], and was used to realise many communication protocols including quantum teleportation [4] and dense coding [14]. More recently high intensity down conversion sources allowed the direct production of three- and four-photon entangled states [28, 9] with which communication protocols involving more than two parties like multiparty secret sharing [30] could be implemented. Stimulated emission in the down conversion process could be used to realise near-optimal quantum cloning of polarisation states of photons [32].

Quantum telecloning is the simultaneous communication of an unknown quantum state to two distant parties and relies on the establishment of a four-particle entangled state.

It represents a combination of quantum teleportation and optimal quantum cloning, since quantum information is copied and transmitted in a single step.

The goal of this diploma thesis was the experimental implementation of quantum telecloning using a four-photon polarisation entangled state, which is obtained directly from parametric down conversion. The state to be telecloned was encoded in the polarisation of a strongly attenuated laser beam approximating single photons.

The experiment posed a challenge in two different respects. On the one hand the detection of a five-photon state was required, which was at the border of feasibility due to extremely low countrates and high background contributions and therefore had no example. On the other hand two photons from independent sources (one from the weak coherent beam and one from down conversion) had to be projected onto the Bell state basis. The establishment and optimisation of the necessary quantum interference was one of the main tasks of my work during this year.

As a preliminary study a teleportation experiment was planned which required the same experimental setup but shorter measurement times.

The experiment has been performed together with two PhD students, Sascha Gaertner, who had also planned and prepared the experiment, and Nikolai Kiesel, who joined us later on and is now taking over the experimental work.

The thesis is organised as follows. Chapter 2 provides the theoretical basis for the experiment. It is shown how qubits, the basic unit of quantum information, can be encoded in polarisation states of photons, and a definition of entanglement is given. It follows the theory of quantum teleportation, optimal quantum cloning and quantum telecloning. In chapter 3 different techniques necessary for the implementation of the scheme are presented: the process of parametric down conversion with which polarisation entangled two- and four-photon states were generated, interferometric Bell state analysis, and a method for the measurement of density matrices of qubits, which was used for an analysis of the output states. Finally in chapter 4 the experimental procedures and results are presented.

2 Theory

In this chapter the theoretical basis for the experiment is provided. It starts with a description of the different forms of polarisation of light in section 2.1. The polarisation of a light wave is oriented perpendicular to the propagation direction and therefore can always be decomposed in two orthogonal polarisation components. Hence the polarisation state of a single photon is a two level quantum system which can be used to encode qubits, the basic unit of quantum information, as described in section 2.2.

Like many quantum communication schemes quantum telecloning relies on entanglement between qubits, which is introduced in section 2.3. Since quantum telecloning represents a combination of quantum teleportation and optimal quantum cloning [1], chapters 2.4 and 2.5 deal with those two subjects. Quantum teleportation is the transmission and reconstruction of an unknown quantum state over arbitrary distances [3, 4], and optimal quantum cloning is the most faithful way to copy quantum information [11, 5, 2], since perfect copying is forbidden by the no-cloning theorem [10]. In the process of quantum telecloning two optimal clones of an unknown quantum state are transferred to two distant receivers. The scheme is presented in section 2.6.

2.1 Polarised light

A light wave can be described as an oscillating electromagnetic field. It is called polarised if the field directions are periodic functions of time and space as opposed to unpolarised light where these directions vary randomly [25]. Because the magnetic field is always oriented perpendicularly to the electric field one usually considers only the electric field. For polarised light propagating along the z axis the electric field can always be decomposed in a field in x direction and a field in y direction:

$$\begin{aligned}\vec{E}_x(z, t) &= E_x \vec{e}_x \sin(\omega t - kz + \phi_1) \\ \vec{E}_y(z, t) &= E_y \vec{e}_y \sin(\omega t - kz + \phi_2)\end{aligned}$$

If both components are in phase the light is called **linearly polarised**:

$$\vec{E}(z, t) = (E_x \vec{e}_x + E_y \vec{e}_y) \sin(\omega t - kz + \phi_0)$$

If they have the same magnitude but a relative phase shift of $\pi/2$ the light is called left or right **circularly polarised**:

Right circular polarisation (rcp):

$$\vec{E}_{rcp}(z, t) = E(\sin(\omega t - kz + \phi_0)\vec{e}_x + \cos(\omega t - kz + \phi_0)\vec{e}_y)$$

Left circular polarisation (lcp):

$$\vec{E}_{lcp}(z, t) = E(\sin(\omega t - kz + \phi_0)\vec{e}_x - \cos(\omega t - kz + \phi_0)\vec{e}_y)$$

For all other combinations of \vec{E}_x and \vec{E}_y the light is called **elliptically polarised**. Instead of \vec{E}_x and \vec{E}_y one can also choose \vec{E}_{rcp} and \vec{E}_{lcp} as a basis, i.e. every polarisation can be written as a combination of left and right circularly polarised light.

The different forms of polarisations can be represented by the points on the surface of the Poincaré sphere as shown in Fig. 2.1. The points on the equator represent linear polarisations where H and V stand for horizontal and vertical polarisation, the north and south poles represent circular polarisation and all other points represent elliptical polarisations.

The transformation of one polarisation state to another can be done by changing the relative phase shift of two orthogonal polarisation components. This can be realised by the use of retarder plates consisting of birefringend material. With a combination of a half and a quarter wave plate any possible transformation can be implemented.

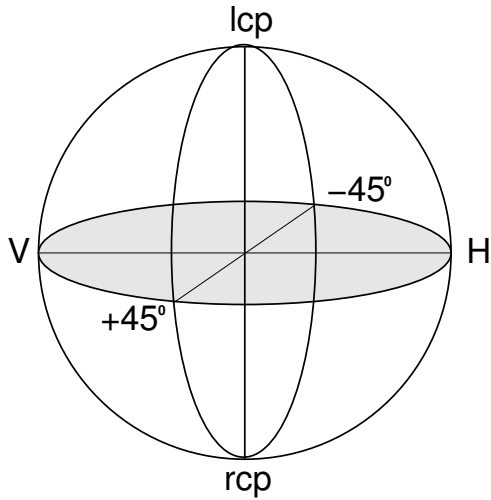


Figure 2.1: Poincaré sphere

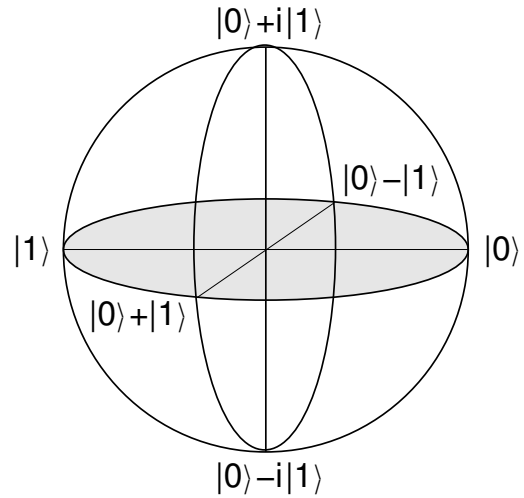


Figure 2.2: Bloch sphere

2.2 Qubits

The basic unit of classical information is called a bit, which is a number with the two possible values 0 and 1. Bits can be encoded in any system with two distinguishable

states, for example two different voltages between the plates of a capacitor.

A qubit is the quantum analog of a bit. It is also a two-state system with the states $|0\rangle$ and $|1\rangle$. But unlike a classical bit a qubit can also be in any coherent superposition state

$$|Q\rangle = \alpha|0\rangle + \beta|1\rangle \quad \text{with} \quad |\alpha|^2 + |\beta|^2 = 1.$$

There are many different possibilities of encoding qubits, in principle any quantum system with at least two states can be used, for example two electronic states of an atom or the two spin states of a spin $\frac{1}{2}$ particle. For the experiment described in this thesis the two polarisation degrees of freedom of photons are used. With the relation

$$\begin{aligned} |H\rangle &\leftrightarrow |0\rangle \\ |V\rangle &\leftrightarrow |1\rangle \end{aligned}$$

the Poincare sphere can be transformed into the Bloch sphere, representing the Hilbert space of a qubit, as shown in Fig. 2.2.

The polarisation degree of freedom has the same algebra as a spin. There are three conjugate bases which are commonly used to describe the polarisation state of a photon:

- HV-basis: $\{|H\rangle, |V\rangle\}$ horizontal and vertical polarisation
- 45°-basis: $\{|+\rangle, |-\rangle\}$ linear polarisation with the polarisation axis at $+45^\circ$ and -45° relative to the horizontal axis.
- LR-basis: $\{|L\rangle, |R\rangle\}$ left circular and right circular polarisation

2.3 Entanglement

In systems containing more than one qubit there can be correlations between the different states, called entanglement, which are much stronger than any classical correlation could be. For example in a maximally entangled two-qubit system the result of a measurement of one of the qubits can exactly predict the state of the unobserved second qubit not only in a particular measurement basis but in every possible basis, while the state of the single qubits is completely undefined. The whole information carried by such an entangled system is encoded in the correlation between the qubits while a single qubit contains no information.

For many years entanglement has just been seen as one of those puzzling features of quantum mechanics, but in the relatively new field of quantum information theory entanglement is used as resource for communication for example in quantum teleportation [3, 4], quantum cryptography [15] or dense coding [13, 14].

Entanglement is defined as follows.

- **Pure states:** The state $|\psi\rangle \in \mathcal{H} = \mathcal{H}_1 \otimes \mathcal{H}_2 \otimes \cdots \otimes \mathcal{H}_N$ of a composite system consisting of N subsystems is called **separable** if it can be written as a tensor product

$$|\psi\rangle = |\psi\rangle_1 \otimes |\psi\rangle_2 \otimes \cdots \otimes |\psi\rangle_N$$

with $|\psi\rangle_1 \in \mathcal{H}_1, |\psi\rangle_2 \in \mathcal{H}_2, \dots, |\psi\rangle_N \in \mathcal{H}_N$.

If this is not possible the state is called **entangled**.

- **Mixed states:** The state $\rho \in \mathcal{B}(\mathcal{H}) = \mathcal{B}(\mathcal{H}_1) \otimes \mathcal{B}(\mathcal{H}_2) \otimes \dots \otimes \mathcal{B}(\mathcal{H}_N)$ is called **separable** if it can be written in the form

$$\rho = \sum_k p_k |1_k\rangle\langle 1_k| \otimes |2_k\rangle\langle 2_k| \otimes \dots \otimes |N_k\rangle\langle N_k|$$

with $|1_k\rangle \in \mathcal{H}_1, |2_k\rangle \in \mathcal{H}_2, \dots, |N_k\rangle \in \mathcal{H}_N$

and where $\mathcal{B}(\mathcal{H})$ is the space of bounded operators acting on \mathcal{H} .

Otherwise the state is called **entangled**.

The best known example for entangled states in the case of two qubit systems are the **Bell states**:

$$\begin{aligned} |\phi^+\rangle &= \frac{1}{\sqrt{2}}(|HH\rangle + |VV\rangle) \\ |\phi^-\rangle &= \frac{1}{\sqrt{2}}(|HH\rangle - |VV\rangle) \\ |\psi^+\rangle &= \frac{1}{\sqrt{2}}(|HV\rangle + |VH\rangle) \\ |\psi^-\rangle &= \frac{1}{\sqrt{2}}(|HV\rangle - |VH\rangle) \end{aligned}$$

They form an orthonormal basis of the two qubit Hilbertspace and they are maximally entangled, which means that the reduced density matrices of the single qubit states (which are obtained by tracing over the state of the second qubit) are maximally mixed.

2.4 Quantum teleportation

Quantum teleportation is the transmission of an unknown quantum state between two spatially separated parties. Instead of directly sending the particle carrying the quantum state an auxiliary pair of entangled particles is used to transmit the information. In this way quantum information can be transferred over arbitrary long distances without worrying about losses or noise [4].

The scheme of teleportation is presented here for a pure polarisation state of a photon as input state, but it also works for mixed or entangled states and it can be generalized to systems with more than two orthogonal states [3].

The two parties, Alice and Bob, initially share a pair of maximally entangled photons, for example the Bell state

$$|\psi^-\rangle_{23} = \frac{1}{\sqrt{2}}(|HV\rangle_{23} - |VH\rangle_{23}).$$

Let the initial state which Alice wants to teleport to Bob be

$$|\psi_x\rangle_1 = \alpha|H\rangle_1 + \beta|V\rangle_1,$$

then the state of the three photons is the product state

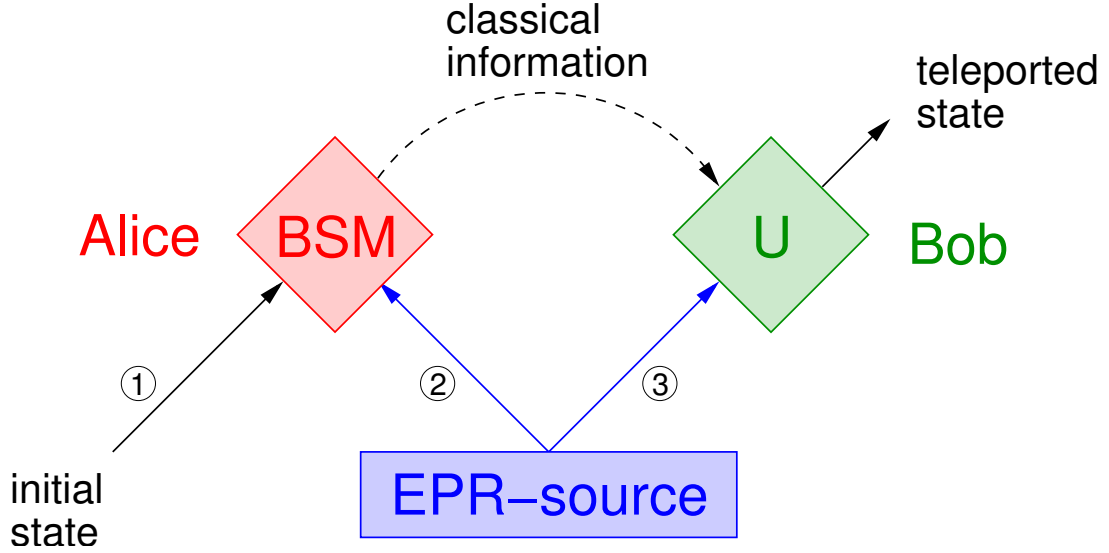


Figure 2.3: The teleportation scheme

$$\begin{aligned} |\psi\rangle_{123} &= |\psi_x\rangle_1 |\psi^-\rangle_{23} \\ &= \frac{\alpha}{\sqrt{2}} (|HHV\rangle_{123} - |HVV\rangle_{123}) \\ &\quad + \frac{\beta}{\sqrt{2}} (|VHV\rangle_{123} - |VVH\rangle_{123}). \end{aligned}$$

The state can be rewritten by expressing each product state of photons 1 and 2 in terms of the Bell basis:

$$\begin{aligned} |\psi\rangle_{123} &= \frac{1}{2} [|\phi^+\rangle_{12} (\alpha|V\rangle_3 - \beta|H\rangle_3) \\ &\quad + |\phi^-\rangle_{12} (\alpha|V\rangle_3 + \beta|H\rangle_3) \\ &\quad - |\psi^+\rangle_{12} (\alpha|H\rangle_3 - \beta|V\rangle_3) \\ &\quad - |\psi^-\rangle_{12} (\alpha|H\rangle_3 + \beta|V\rangle_3)]. \end{aligned}$$

Alice performs a Bell-state measurement on photon 1 and 2, which means that she projects the state of those two photons onto the Bell basis. All four measurement outcomes occur with the same probability $\frac{1}{4}$ and the state of the third photon will be in the corresponding pure state. If Alice detects the Bell-state $|\psi^-\rangle$ Bob's photon is already in the state

$|\psi_x\rangle$ which Alice sought to teleport. In all other cases the state of Bobs photon can be transformed unitarily into the initial state:

$$\begin{aligned} -\sigma_z\sigma_x(\alpha|V\rangle_3 - \beta|H\rangle_3) &= |\psi_x\rangle \\ \sigma_x(\alpha|V\rangle_3 + \beta|H\rangle_3) &= |\psi_x\rangle \\ \sigma_z(\alpha|H\rangle_3 - \beta|V\rangle_3) &= |\psi_x\rangle \end{aligned}$$

with the Pauli matrices

$$\sigma_x = \begin{pmatrix} 0 & 1 \\ 1 & 0 \end{pmatrix} \quad \text{and} \quad \sigma_z = \begin{pmatrix} 1 & 0 \\ 0 & -1 \end{pmatrix}.$$

If Alice sends the result of her Bell-state measurement to Bob by means of classical communication, Bob can apply the corresponding unitary transformation in order to convert the state of his photon into Alice's original state. Whereas photon 1, which was initially in the transferred state, has been projected together with photon 2 onto a maximally entangled state and is therefore in a completely mixed state which doesn't contain any information about the original state.

It is interesting to mention that the teleported quantum information has been split into two parts during the transmission: a purely nonclassical part which is transferred instantaneously via the entanglement between photon 2 and 3, and a purely classical part, the outcome of the Bell-state measurement which is simply a number between 0 and 3 and therefore equals two bit of classical information. The quantum information alone would be of no use, because without the correct unitary transformation the state of photon 3 is in a mixed state which has no correlations with the initial state. Thus the complete teleportation cannot proceed faster than light as required by the principle of causality.

2.5 Quantum cloning

Unlike classical information quantum information cannot be copied with arbitrary precision, this is the message of the no-cloning theorem [10]. There exists an upper bound for the quality of the copies of an arbitrary unknown quantum state which can be reached by a process called optimal quantum cloning [2]. Even if these quantum clones are not perfect, it is impossible to achieve the same quality by just doing a measurement on the input state, which is the usual method to copy classical information.

2.5.1 No-cloning theorem

The no-cloning theorem states that it is impossible to create a perfect copy of an arbitrary unknown quantum state while preserving the original quantum state. For example in quantum teleportation the input state can be recreated perfectly, but just at the expense of the complete destruction of the original state.

The assumption of the existence of such a perfect cloning machine leads to a contradiction

with the linearity of quantum mechanics: Such a machine should produce perfect copies of every quantum state $|\psi\rangle$:

$$|\psi\rangle|0\rangle \xrightarrow{CM} |\psi\rangle|\psi\rangle,$$

for example $|H\rangle$ and $|V\rangle$

$$\begin{aligned} |H\rangle|0\rangle &\xrightarrow{CM} |H\rangle|H\rangle \\ |V\rangle|0\rangle &\xrightarrow{CM} |V\rangle|V\rangle. \end{aligned}$$

The linearity of quantum mechanics implies then:

$$(|H\rangle + |V\rangle)|0\rangle \xrightarrow{QM} |H\rangle|H\rangle + |V\rangle|V\rangle,$$

which is not equivalent to the output of an ideal cloning machine:

$$\begin{aligned} (|H\rangle + |V\rangle)|0\rangle &\xrightarrow{CM} (|H\rangle + |V\rangle)(|H\rangle + |V\rangle) \\ &= |H\rangle|H\rangle + |H\rangle|V\rangle + |V\rangle|H\rangle + |V\rangle|V\rangle. \end{aligned}$$

The no-cloning theorem is one of the most fundamental differences between quantum and classical information theory. For example for a quantum computer it would be impossible to copy data, which is quite a basic task for a classical computer. On the other hand this theorem is the reason for the security of quantum cryptography. Quantum cryptography is based on the fact that it is impossible for an eavesdropper to read the transferred data without disturbing it. If perfect cloning would be possible, an eavesdropper could just create two copies of each qubit, keep one of them and send the other one to the receiver who would have no possibility to find out about the eavesdropping.

2.5.2 Optimal quantum cloning

Perfect cloning is impossible according to the no-cloning theorem, but it is interesting to ask how accurately such copies can be made. As a measurement for the quality of the copies the **fidelity** F is used. It is defined as the mean overlap between a copy and the input state:

$$F := \langle \psi_x | \rho_c | \psi_x \rangle$$

where $|\psi_x\rangle$ is the input state and ρ_c is the density matrix of one of the copies. The fidelity is a number between 0 and 1, 1 for a perfect copy $\rho_c = |\psi_x\rangle\langle\psi_x|$ and 0 if the output state is orthogonal to the input state.

The process of cloning quantum states can be described by a **quantum cloning machine** [2] which transforms N identical qubits into $M > N$ identical copies. The initial state, consisting of N input qubits, $M - N$ so called blank paper qubits and an ancilla, is transformed unitarily into the state of M clones and the ancilla. It can be shown [2] that the maximal fidelity of the clones achievable in such a process is

$$F_{N,M} = \frac{M(N+1) + N}{M(N+2)}. \quad (2.1)$$

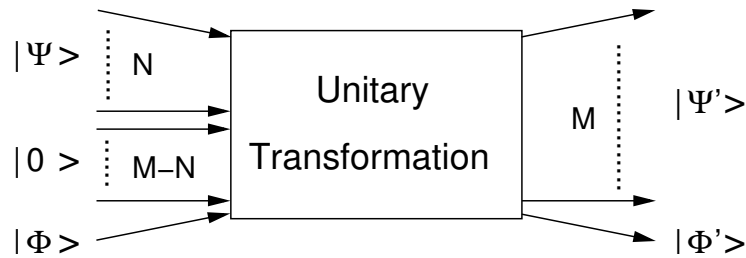


Figure 2.4: Quantum cloning machine

If the quality of the copies is dependent on the input state it is possible to reach higher fidelities for some particular input states. For example the copying machine considered in the proof of the no-cloning theorem works perfectly for the input states $|H\rangle$ and $|V\rangle$ but creates poor copies of some superpositions of $|H\rangle$ and $|V\rangle$. If this maximal fidelity (Eq. (2.1)) is reached for all kinds of input states then the process is called optimal universal quantum cloning.

The more input states there are the more information is given about them, in the case of a quasiclassical input state with $N \rightarrow \infty$ and $M = N + 1$ the fidelity tends towards 1. On the other hand the fidelity of the copies decreases if their number M grows, corresponding to the fact that the information is spread among a bigger number of parties.

For the telecloning experiment described in this thesis two copies of a single qubit have been made, so the optimal fidelity in this case would be

$$F_{1,2} = \frac{5}{6} \approx 83,3\%.$$

2.5.3 The 'classical' limit

The quantum cloning machine can be compared with a simpler copying process which is called the **classical copying machine**. It consists in a measurement on the N identical

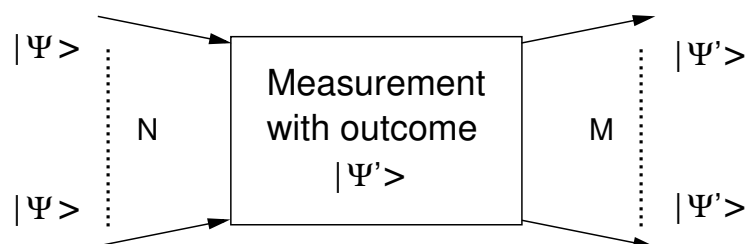


Figure 2.5: Classical copying machine

input states and the result of the measurement is used to make an arbitrary number M of copies. It can be shown [18] that in this case the maximal (average) fidelity, which is often

referred to as the classical limit, is

$$F_N = \frac{N+1}{N+2}.$$

It is of course independent of the number of copies which are made, and it also tends towards 1 for a quasiclassical input state with $N \rightarrow \infty$.

This maximum fidelity can be reached by so called optimal measurements where the input qubits are not measured separately but as a single composite system [18]. In the case of a single qubit an optimal measurement is just a projection onto two (randomly chosen) orthogonal states.

For example the polarisation state of a photon could be projected onto the HV-basis. Suppose the photon is in the polarisation state $|H\rangle$, then the outcome of the measurement would always be $|H\rangle$ and therefore the fidelity would be 1. But if the measurement is done in the 45-basis the outcome would be $|+\rangle$ or $|-\rangle$ with equal probability which both give a fidelity of $\frac{1}{2}$ and the same is true for a measurement in the LR-basis. Thus the average fidelity achieved by such a projection measurement is

$$F = \frac{2}{3} \approx 66,7\%,$$

which is the classical limit in the case of $N = 1$.

Apparently the fidelity achievable with an optimal cloning process is always higher than the classical limit for the same number of input states. Just in the limit of infinitely many copy states the two fidelities get equal, meaning that the quantum cloning machine tends towards the classical copying machine.

2.6 Quantum telecloning

Quantum telecloning combines quantum teleportation and optimal quantum cloning in such a way that $M > 1$ optimal clones of an unknown quantum state are created and distributed among distant parties. In principle this could be done by first creating optimal clones of the input state and teleporting these copies to the recipients. But the amount of entanglement needed for the telecloning protocol is much lower as shown in [1]. By using a multiparticle entangled state all copies can be transmitted simultaneously by means of a single measurement.

In the experiment presented in this thesis $M = 2$ copy states have been created, therefore only this case will be considered here (for the general case see [1]).

The situation is as follows. Alice holds the original quantum state $|\psi_x\rangle$ which she wishes to teleclone to two distant associates, Charlie and Claire.

$$|\psi_x\rangle_1 = \alpha|H\rangle_1 + \beta|V\rangle_1$$

As a starting resource the three parties have to share a four-photon entangled state, the so called telecloning state $|\psi_{TC}\rangle$.

$$\begin{aligned} |\psi_{TC}\rangle_{2345} &= \frac{1}{\sqrt{3}} \left[|HHHH\rangle + |VVVV\rangle \right. \\ &\quad \left. + \frac{1}{2} (|HVHV\rangle + |VHVH\rangle \right. \\ &\quad \left. + |HVVH\rangle + |VHHV\rangle) \right]_{2345} \end{aligned}$$

Photon 2 is on Alice's side, photon 3 serves as an ancilla and photons 4 and 5 are distributed to Charly and Claire. Due to the high symmetry of the telecloning state the roles of photons 2 and 3 or 4 and 5 can be exchanged. Also 2 and 3 together can be exchanged with 4 and 5. This implies that any of the four locations can be used as the sending port and that both receivers will obtain exactly the same information.

The state of all five photons is the product state

$$\begin{aligned} |\psi\rangle_{12345} &= |\psi_x\rangle_1 |\psi_{TC}\rangle_{2345} \\ &= \frac{\alpha}{\sqrt{3}} \left[|HHHHH\rangle + |HVVVV\rangle \right. \\ &\quad \left. + \frac{1}{2} (|HHVHV\rangle + |HVHVH\rangle + |HHV VH\rangle + |HVHHV\rangle) \right] \\ &\quad + \frac{\beta}{\sqrt{3}} \left[|VHHHH\rangle + |VVVVV\rangle \right. \\ &\quad \left. + \frac{1}{2} (|VHVHV\rangle + |VVHVH\rangle + |VHV VH\rangle + |VVHHV\rangle) \right]_{12345}. \end{aligned}$$

As for the teleportation (see section 2.4) this can be rewritten by expressing all product states of photon 1 and 2 in terms of the Bell basis:

$$\begin{aligned} |\psi\rangle_{12345} &= \frac{1}{2} \left[|\phi^+\rangle_{12} |\chi\rangle_{345} \right. \\ &\quad \left. + |\phi^-\rangle_{12} \sigma_z \otimes \sigma_z \otimes \sigma_z |\chi\rangle_{345} \right. \\ &\quad \left. + |\psi^+\rangle_{12} \sigma_x \otimes \sigma_x \otimes \sigma_x |\chi\rangle_{345} \right. \\ &\quad \left. + |\psi^-\rangle_{12} \sigma_z \sigma_x \otimes \sigma_z \sigma_x \otimes \sigma_z \sigma_x |\chi\rangle_{345} \right] \end{aligned}$$

with

$$\begin{aligned} |\chi\rangle_{345} &= \sqrt{\frac{2}{3}} \left[a (|HHH\rangle + \frac{1}{2} (|VVH\rangle + |VHV\rangle)) \right. \\ &\quad \left. + b (|VVV\rangle + \frac{1}{2} (|HHV\rangle + |HVH\rangle)) \right]_{345}. \end{aligned}$$

Alice performs a Bell state measurement on photons 1 and 2 after which the state of the remaining 3 photons is either $|\chi\rangle$ or some unitary transformation of $|\chi\rangle$. This state is a

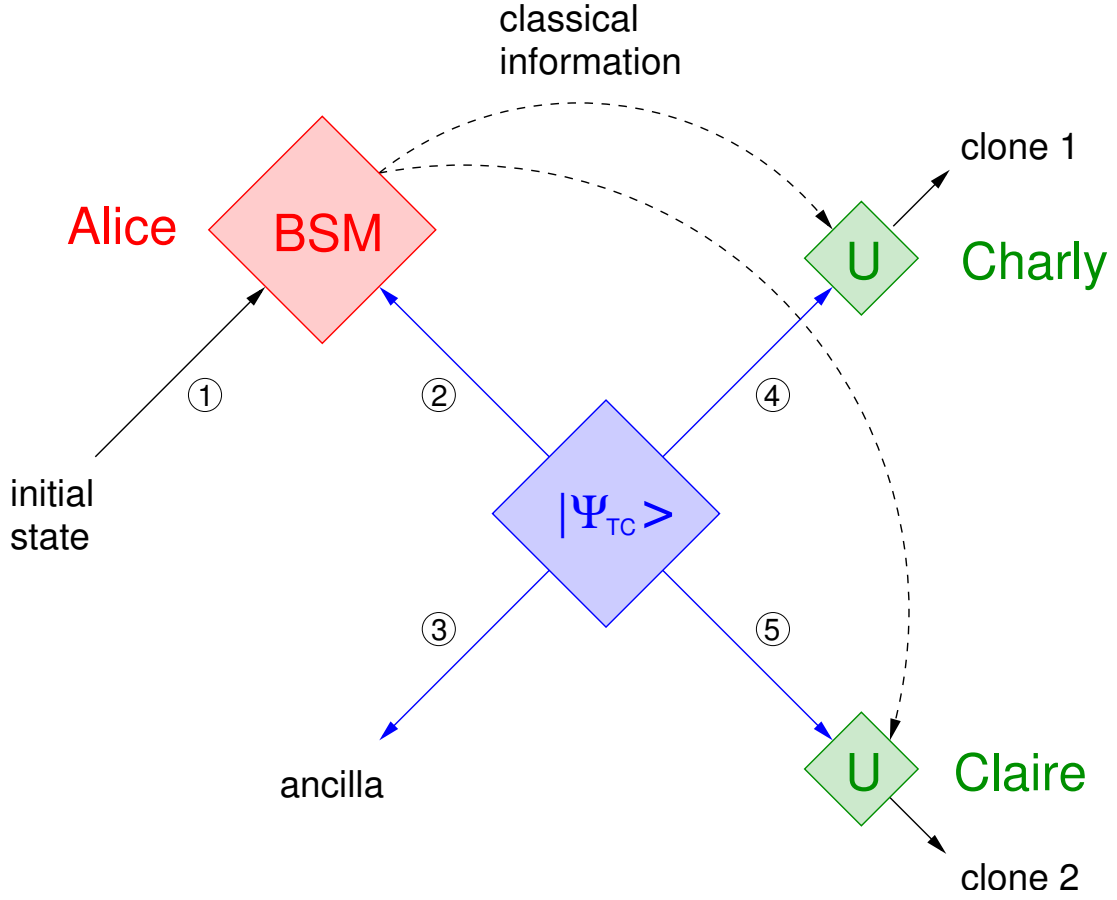


Figure 2.6: The telecloning scheme

three-photon entangled state of the ancilla photon and two optimal clones of the input state as will be shown below. If Alice detects $|\phi^+\rangle$ photons 4 and 5 are already in the desired state, if she detects one of the other three Bell states Charly and Claire have to perform the appropriate unitary transformation on their photons to obtain two optimal quantum clones. Like in the teleportation protocol the outcome of the Bell state measurement is sent to Charly and Claire via classical communication.

To show that photons 4 and 5 are really in the optimal cloning state their fidelity with respect to the input state has to be calculated. The reduced density matrices of the two states are

$$\begin{aligned}
 \rho_4 &= \text{tr}_{3,5}(|\chi\rangle_{345}\langle\chi|) \\
 \rho_5 &= \text{tr}_{3,4}(|\chi\rangle_{345}\langle\chi|) \\
 \rho_4 = \rho_5 &= \frac{1}{6} \begin{pmatrix} 5|a|^2 + |b|^2 & 2(ab^* + a^*b) \\ 2(ab^* + a^*b) & 5|b|^2 + |a|^2 \end{pmatrix} \\
 &= F|\psi_x\rangle\langle\psi_x| + (1-F)|\psi_x^\perp\rangle\langle\psi_x^\perp|,
 \end{aligned}$$

where F is the fidelity to the input state $|\psi_x\rangle$ given by

$$\begin{aligned} F &= \langle \psi_x | \rho_{4,5} | \psi_x \rangle \\ &= \begin{pmatrix} a^* & b^* \end{pmatrix} \frac{1}{6} \begin{pmatrix} 5|a|^2 + |b|^2 & 2(ab^* + a^*b) \\ 2(ab^* + a^*b) & 5|b|^2 + |a|^2 \end{pmatrix} \begin{pmatrix} a \\ b \end{pmatrix} \\ &= \frac{5}{6}, \end{aligned}$$

which is the maximum for a $N = 1 \rightarrow M = 2$ cloning process as shown in Eq. (2.1).

Entanglement structure during the telecloning process

Before the Bell state measurement the state is a direct product of the input state $|\psi_x\rangle$ and the four-photon entangled telecloning state $|\psi_{TC}\rangle$. The telecloning state is a superposition of a four-photon GHZ state and a product of two Bell states [8, 9]

$$|\psi_{TC}\rangle = \sqrt{\frac{2}{3}}|GHZ\rangle_{2345} + \sqrt{\frac{1}{3}}|\psi^+\rangle_{23}|\psi^+\rangle_{45}$$

with the GHZ-term

$$|GHZ\rangle = \frac{1}{\sqrt{2}}(|HHHH\rangle + |VVVV\rangle)$$

and the Bell state

$$|\psi^+\rangle = \frac{1}{\sqrt{2}}(|HV\rangle + |VH\rangle).$$

The Bell state measurement projects the state of photon 1 and 2 onto a maximally



Figure 2.7: Entanglement structure before and after the Bell state measurement. The solid lines indicate 2-photon entanglement.

entangled state and the remaining 3 photons are left in the state $|\chi\rangle$ which is a three-photon entangled state of the W-class [6].

The two-photon entanglement between Alice's photon and the photons of the recipients is of course necessary for the transmission of information, but after the Bell state measurement there exists also two-photon entanglement between the two clones [1, 6]. Their reduced

two photon density matrix is

$$\rho_{45} = \text{tr}_3(|\chi\rangle_{345}\langle\chi|) = \frac{2}{3} \begin{pmatrix} |a|^2 & \frac{ab^*}{2} & \frac{ab^*}{2} & 0 \\ \frac{a^*b}{2} & \frac{1}{4} & \frac{1}{4} & \frac{ab^*}{2} \\ \frac{a^*b}{2} & \frac{1}{4} & \frac{1}{4} & \frac{ab^*}{2} \\ 0 & \frac{a^*b}{2} & \frac{a^*b}{2} & |b|^2 \end{pmatrix}. \quad (2.2)$$

Because the telecloning process is universal it is sufficient to examine one input state, for example $|\psi\rangle_x = |+\rangle$. For $a = b = \frac{1}{\sqrt{2}}$ (2.2) becomes

$$\rho_{45} = \frac{2}{3} \begin{pmatrix} \frac{1}{2} & \frac{1}{4} & \frac{1}{4} & 0 \\ \frac{1}{4} & \frac{1}{4} & \frac{1}{4} & \frac{1}{4} \\ \frac{1}{4} & \frac{1}{4} & \frac{1}{4} & \frac{1}{4} \\ 0 & \frac{1}{4} & \frac{1}{4} & \frac{1}{2} \end{pmatrix}. \quad (2.3)$$

According to the Peres-Horodecki theorem [19, 20] the two-photon state is entangled if the partial transpose of the states density matrix has at least one negative eigenvalue. The partial transpose of Eq. (2.3) is

$$\rho_{45}^{T_2} = \frac{2}{3} \begin{pmatrix} \frac{1}{2} & \frac{1}{4} & \frac{1}{4} & \frac{1}{4} \\ \frac{1}{4} & \frac{1}{4} & 0 & \frac{1}{4} \\ \frac{1}{4} & 0 & \frac{1}{4} & \frac{1}{4} \\ \frac{1}{4} & \frac{1}{4} & \frac{1}{4} & \frac{1}{2} \end{pmatrix},$$

with the eigenvalues $\frac{1}{4}, \frac{1}{4}, \frac{1}{4}(2 - \sqrt{5})$ and $\frac{1}{4}(2 + \sqrt{5})$, where the third one is negative, indicating two-photon entanglement between the two clones.

3 Implementation

In this chapter the building blocks for the realisation of the experiment are presented. Two basic techniques of experimental quantum information are introduced, namely the use of parametric down conversion as source of entangled photons in section 3.1, and interferometric Bell state analysis in section 3.2.

The chapter starts with the description of the type-II spontaneous parametric down conversion process which was used for the generation of two- and four-photon entangled states [7, 9]. Two-photon states are obtained from first order emissions and were used to perform quantum teleportation, while the four-photon states used for the implementation of quantum telecloning originate from second order emissions. In the latter case a postselection of events is necessary.

Both teleportation and telecloning required the projection of a weak coherent state and one of the down conversion photons onto the Bell state basis. An interferometric method was applied with which two of the four Bell states can be identified [21]. The necessary overlap at a beam splitter was aligned by utilizing a two-photon interference effect, the so called Hong Ou Mandel dip [16]. The visibility of this dip provides a measure of quality for the Bell state analysis. Furthermore the influence of beam splitter parameters, like transmissivity and reflectivity of different polarisations as well as phase shifts, on the Bell state analysis have been studied. For the case of phase shifts the possibilities of compensation are discussed.

In section 3.3 it is explained how density matrices of photon states can be measured. This technique was used for the analysis of the output states of the telecloning process.

3.1 Parametric down conversion

Type-II noncollinear phase matching in spontaneous parametric down conversion (SPDC) allows the direct production of polarisation entangled photons out of a nonlinear crystal [7]. In the process of down conversion a pump photon decays into two daughter photons. Due to dispersion the momentum conservation can only be fulfilled in birefringent crystals, in our setup we used BBO (beta-barium borate). In type-II SPDC the pump beam has ordinary polarisation and the two emerging photons, called signal and idler photon, have extraordinary and ordinary polarisation respectively. Due to the conservation of energy

and momentum, i. e.

$$\begin{aligned}\hbar\omega_{pump} &= \hbar\omega_{signal} + \hbar\omega_{idler} \\ \hbar\vec{k}_{pump} &= \hbar\vec{k}_{signal} + \hbar\vec{k}_{idler}\end{aligned}$$

the photons must be emitted on opposite sides of the pump beam, with the possible emission directions forming two cones. Depending on the angle between pump beam direction

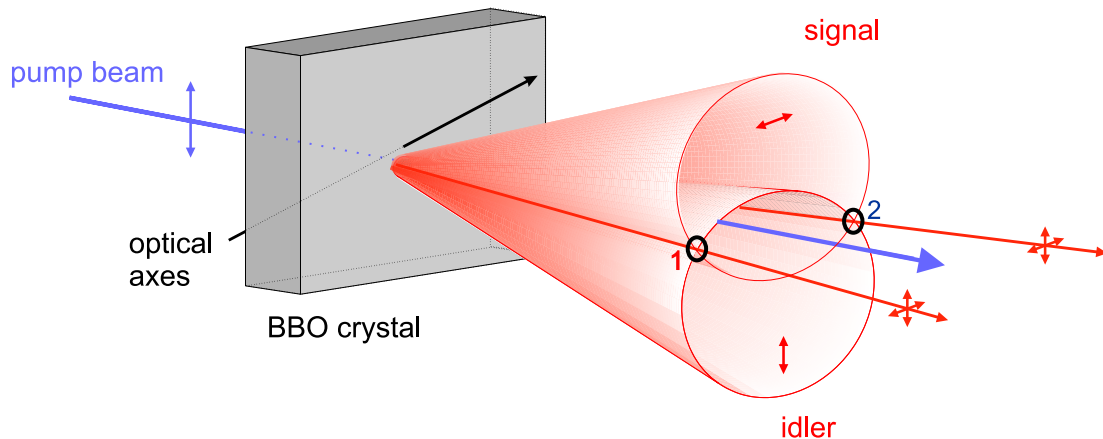


Figure 3.1: Type-II SPDC

and optical axis the cones can either be completely separated, be tangent to each other (collinear case) or exhibit two intersection lines as shown in Fig. 3.1. If both photons have the same wavelength (degenerate case) those intersection lines yield entangled photons. The polarisation of photons emitted in those directions is completely undefined but if one photon is horizontally polarised the second one will be vertically polarised and the other way round. The selection of those two spatial modes is done by the coupling into single mode optical fibers. The longitudinal and transverse walk-off between the two polarisations caused by the birefringence of the crystal renders the two different emissions in principle distinguishable. In order to observe entanglement this walk-off has to be compensated by the use of two extra birefringent crystals.

Four-photon entanglement from down-conversion

If the intensity of the pump beam is high enough, in our setup we use 700mW of pulsed UV-light, there is a reasonable probability of creating two down-converted pairs simultaneously. Due to interference this second order process leads to the emission of a four-photon entangled state if the coherence length of the photons exceeds the pulse length. The coherence length is proportional to the inverse of the spectral width and therefore can be manipulated by interference filters. We used 3nm filters in front of the coupling into single mode fibers. The full state emitted into the two intersection directions a_0 and b_0 (see Fig.3.2) is [8]

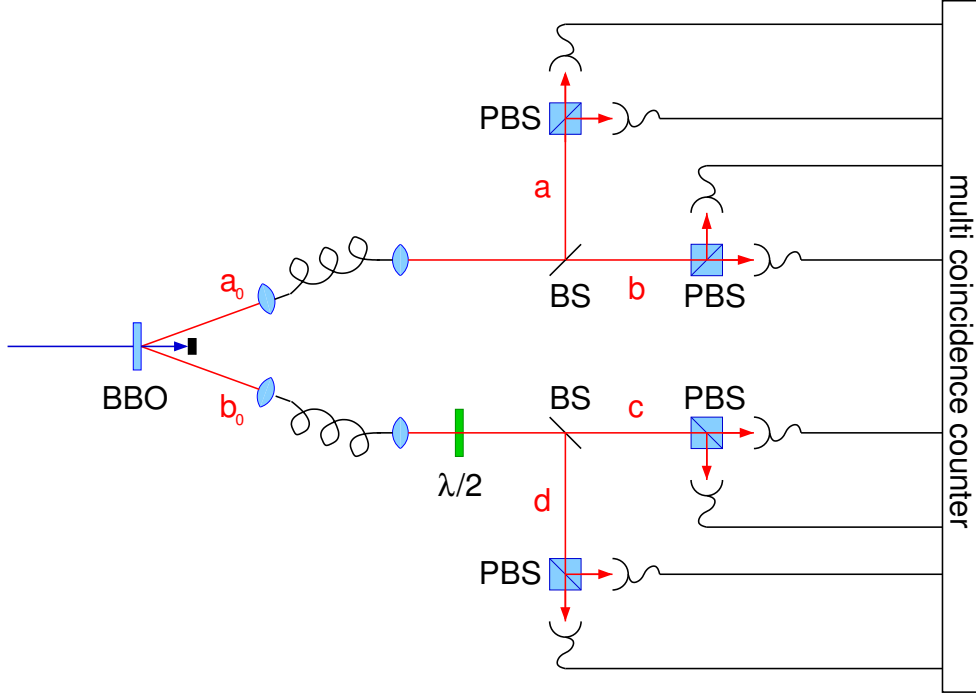


Figure 3.2: Experimental setup to generate the four-photon polarisation entangled state

$$\begin{aligned}
 |\psi_{DC}\rangle &= Z \exp[-ic(a_{0V}^\dagger b_{0H}^\dagger + a_{0H}^\dagger b_{0V}^\dagger)]|0\rangle \\
 &= Z(|0\rangle - \underbrace{ic(a_{0H}^\dagger b_{0V}^\dagger + a_{0V}^\dagger b_{0H}^\dagger)}_{2 \text{ photons}}|0\rangle - \underbrace{\frac{c^2}{2}(a_{0H}^\dagger b_{0V}^\dagger + a_{0V}^\dagger b_{0H}^\dagger)^2}_{4 \text{ photons}}|0\rangle) \\
 &\quad + \text{higher-order-terms},
 \end{aligned} \tag{3.1}$$

where c is a constant proportional to the pump intensity, Z is a normalisation constant and a_{0V}^\dagger is the creation operator of a vertically polarised photon in mode a_0 , etc. The first order term corresponds to the emission of a two-photon entangled state, namely the Bell state

$$(a_{0H}^\dagger b_{0V}^\dagger + a_{0V}^\dagger b_{0H}^\dagger)|0\rangle = |HV\rangle_{a_0 b_0} + |VH\rangle_{a_0 b_0} = \sqrt{2}|\psi^+\rangle_{a_0 b_0}.$$

By the use of additional birefringent phase shifters any of the four Bell states can be prepared easily, turning type-II SPDC into an important resource for many experiments in the field of quantum information.

For the teleconing experiment the four-photon state given by the second order term is needed. Its expansion is

$$(a_{0H}^\dagger b_{0V}^\dagger + a_{0V}^\dagger b_{0H}^\dagger)^2|0\rangle = (a_{0H}^{\dagger 2} b_{0V}^{\dagger 2} + a_{0V}^{\dagger 2} b_{0H}^{\dagger 2} + 2a_{0H}^\dagger a_{0V}^\dagger b_{0H}^\dagger b_{0V}^\dagger)|0\rangle.$$

This can be written as a superposition of photon number states

$$|2H_{a_0}, 2V_{b_0}\rangle + |2V_{a_0}, 2H_{b_0}\rangle + |1H_{a_0}, 1V_{a_0}, 1H_{b_0}, 1V_{b_0}\rangle,$$

where for example $2H_{a_0}$ means two horizontally polarised photons in mode a_0 (the different representations of photon states are explained in the appendix). To separate the four photons, the two output modes are split up at beam splitters and only those events are selected where one photon is detected in each output mode. The transformation of symmetric 50:50 beam splitter, which will be studied in detail in the next section, is given by

$$a_0^\dagger \rightarrow \frac{1}{\sqrt{2}}(b^\dagger + ia^\dagger) \quad \text{and} \quad b_0^\dagger \rightarrow \frac{1}{\sqrt{2}}(c^\dagger + id^\dagger).$$

The selection of events leads to the following four photon state.

$$\begin{aligned} |\psi^A\rangle_{abcd} = & \frac{1}{\sqrt{3}} \left[|HHVV\rangle + |VVHH\rangle \right. \\ & + \frac{1}{2} (|HVVH\rangle + |VHHV\rangle \\ & \left. + |HVHV\rangle + |VHVH\rangle) \right]_{abcd} \end{aligned}$$

To obtain the telecloning state the polarisation in one arm is rotated either by a half wave plate or by means of the polarisation controllers of the optical fiber.

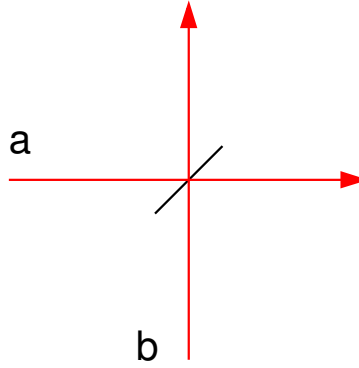
$$\begin{aligned} |\psi_{TC}\rangle_{abcd} = & \frac{1}{\sqrt{3}} \left[|HHHH\rangle + |VVVV\rangle \right. \\ & + \frac{1}{2} (|HVHV\rangle + |VHVH\rangle \\ & \left. + |HVVH\rangle + |VHHV\rangle) \right]_{abcd} \end{aligned}$$

3.2 Bell state analysis

An essential part of the experiment is the projection of two photons onto the Bell state basis. By means of two-photon interference two of the four Bell states can be identified [21], the distinction between all four Bell states is just possible if the photons are entangled in yet another degree of freedom [22]. But for teleportation and telecloning it is sufficient to identify only one Bell state and discard all other detection events, obtaining a successful transfer of the state in one quarter of the trials.

The interferometric Bell state analysis makes use of the fact that $|\psi^-\rangle$ is the only Bell state with an antisymmetric polarisation part of the wave function. Because photons are bosons the whole wave function has to be symmetric, implying an antisymmetric spatial part of the wave function of $|\psi^-\rangle$.

The two photons to be projected onto the Bell state basis are overlapped at a beamsplitter with the two spatial modes a and b . Before entering the beam splitter the complete wave



functions of the four Bell states are:

$$\begin{aligned} |\phi^+\rangle &= \frac{1}{2}(|HH\rangle + |VV\rangle)(|ab\rangle + |ba\rangle) \\ |\phi^-\rangle &= \frac{1}{2}(|HH\rangle - |VV\rangle)(|ab\rangle + |ba\rangle) \\ |\psi^+\rangle &= \frac{1}{2}(|HV\rangle + |VH\rangle)(|ab\rangle + |ba\rangle) \\ |\psi^-\rangle &= \frac{1}{2}(|HV\rangle - |VH\rangle)(|ab\rangle - |ba\rangle). \end{aligned}$$

The transformation matrix of a symmetric beam splitter with reflectivity r^2 and transmissivity t^2 in the $\{|a\rangle, |b\rangle\}$ - basis is

$$\underline{B} = \begin{pmatrix} t & ir \\ ir & t \end{pmatrix}$$

For a 50:50 splitting ratio with $t = r = \frac{1}{\sqrt{2}}$ the basis states transform like

$$|a\rangle \rightarrow \frac{1}{\sqrt{2}}(|a\rangle + i|b\rangle) \quad \text{and} \quad |b\rangle \rightarrow \frac{1}{\sqrt{2}}(|b\rangle + i|a\rangle)$$

Thus the transformations of the spatial parts of the wave functions are

$$\begin{aligned} \frac{1}{\sqrt{2}}(|ab\rangle + |ba\rangle) &\rightarrow \frac{1}{\sqrt{2}}(|aa\rangle + |bb\rangle) \\ \frac{1}{\sqrt{2}}(|ab\rangle - |ba\rangle) &\rightarrow \frac{1}{\sqrt{2}}(|ab\rangle - |ba\rangle) \end{aligned}$$

meaning that for $|\psi^-\rangle$ both photons always leave the beam splitter in different output modes while for the other three Bell states both photons leave the beam splitter in the same output mode, either both in mode a or both in mode b . Therefore the state $|\psi^-\rangle$ can be distinguished from the other Bell states. It is the only one that leads to coincidences between two detectors in the output modes of the beamsplitter.

We can further discriminate between the state $|\psi^+\rangle$ and the states $|\phi^\pm\rangle$ by analysing the polarisation of the photons in the output modes in the HV-basis. If the two photons are in the state $|\psi^+\rangle$ they have different polarisation while in the other two cases they have the same polarisation. The scheme is depicted in Fig. 3.3 where the blue lines mark

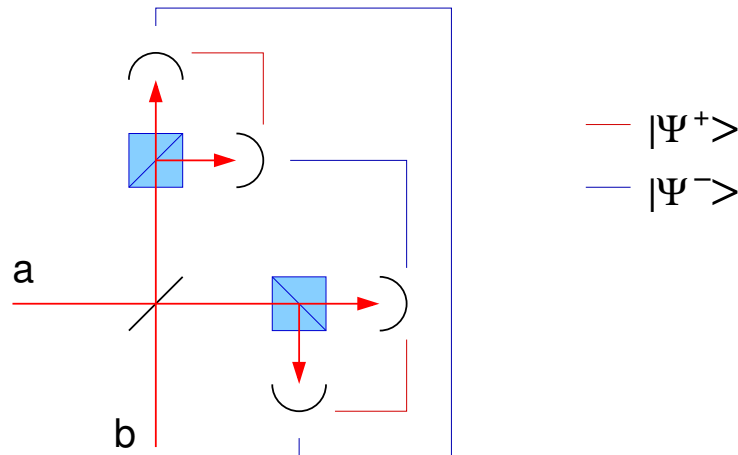


Figure 3.3: Bell state analyser for detecting the states $|\psi^-\rangle$ and $|\psi^+\rangle$

detection coincidences corresponding to the detection of $|\psi^-\rangle$ and the red lines mark those corresponding to $|\psi^+\rangle$.

With setups similar to the one described here any two of the four Bell states can be identified, for example if a PBS is used instead of a BS, it is possible to detect the states $|\phi^+\rangle$ and $|\phi^-\rangle$ [23].

3.2.1 Influences of beam splitter parameters on the Bell state analysis

In the preceding calculations an ideal beamsplitter with a 50:50 splitting ratio for all kinds of polarisations and without any effect on the polarisation has been assumed. But real beamsplitters can have different splitting ratios, maybe even varying with different polarisations or they can introduce phase shifts between two orthogonal polarisation components. In this section the effect of such divergences from the ideal beamsplitter transformation on the Bell state analysis is investigated and it is shown how phase shifts can be compensated. How the beam splitter parameters have been determined is explained in the appendix. The most general transformation matrix of a beamsplitter in the $\{|Ha\rangle, |Hb\rangle, |Va\rangle, |Vb\rangle\}$ -basis, where for example $|Ha\rangle$ means horizontal polarisation in mode a , is given by

$$\underline{B} = \begin{pmatrix} t_{Ha}e^{i\beta_{Ha}} & r_{Hb}e^{i\alpha_{Hb}} & 0 & 0 \\ r_{Ha}e^{i\alpha_{Ha}} & t_{Hb}e^{i\beta_{Hb}} & 0 & 0 \\ 0 & 0 & t_{Va}e^{i\beta_{Va}} & r_{Vb}e^{i\alpha_{Vb}} \\ 0 & 0 & r_{Va}e^{i\alpha_{Va}} & t_{Vb}e^{i\beta_{Vb}} \end{pmatrix}, \quad (3.2)$$

with the following conditions implied by the unitarity of \underline{B} (the conservation of energy):

$$t_{Ha} = t_{Hb} \equiv t_H \quad t_{Va} = t_{Vb} \equiv t_V \quad (3.3)$$

$$r_{Ha} = r_{Hb} \equiv r_H \quad r_{Va} = r_{Vb} \equiv r_V \quad (3.4)$$

$$\alpha_{Ha} - \beta_{Ha} = \pi + \beta_{Hb} - \alpha_{Hb} \quad (3.5)$$

$$\alpha_{Va} - \beta_{Va} = \pi + \beta_{Vb} - \alpha_{Vb}. \quad (3.6)$$

Here t_{Ha}^2 for example is the transmissivity for horizontal polarisation in mode a .

Phase shifts occur if for a particular path the phase factor for H is different from the phase factor for V, i. e.

$$\begin{aligned} \alpha_{Ha} &\neq \alpha_{Va} & \alpha_{Hb} &\neq \alpha_{Vb} \\ \beta_{Ha} &\neq \beta_{Va} & \beta_{Hb} &\neq \beta_{Vb}. \end{aligned}$$

Such phase shifts cause all polarisation states other than $|H\rangle$ or $|V\rangle$ to be rotated. For example if a photon in the state $|+\rangle$ enters the beamsplitter in arm a and is reflected in arm b the transformation is

$$|+\rangle = \frac{1}{\sqrt{2}}(|H\rangle + |V\rangle) \quad \rightarrow \quad \frac{1}{\sqrt{2}}e^{i\alpha_{Ha}}(|H\rangle + e^{i(\alpha_{Va} - \alpha_{Ha})}|V\rangle),$$

which results in elliptical polarisation.

Special case: no phase shifts in the transmitted beams

The beamsplitters we used didn't show any phase shifts in the transmitted beams, just as one would expect since they are made of non-birefringent material (BK7 glass with a dielectric beam splitter coating). This means

$$\beta_{Ha} = \beta_{Va} \quad \text{and} \quad \beta_{Hb} = \beta_{Vb},$$

and Eqs. (3.5), (3.6) reduce to

$$\alpha_{Ha} - \alpha_{Va} = -(\alpha_{Hb} - \alpha_{Vb}) \equiv \Delta\alpha. \quad (3.7)$$

Thus the absolute values of the phase shifts in both reflected beams are the same and in this case only two retarder plates are necessary for the compensation as shown in Fig. 3.4. The effect of such a phase shift on the Bell state analysis can be calculated by inserting the conditions (3.3), (3.4) and (3.7) in the beamsplitter matrix (3.2) and applying this beamsplitter transformation on the Bell states. Then for every state the probability for the two photons to split up at the beamsplitter can be calculated and plotted against the phase shift $\Delta\alpha$. In Figure 3.6 those probabilities are plotted against the phase shift $\Delta\alpha$ for 3 different values of the transmissivities t_H^2 and t_V^2 . The case where the state $|\psi^-\rangle$ always splits up and all other Bell states don't, appears only if $\Delta\alpha = 2n\pi$ and $t_H^2 = t_V^2 = 0.5$. For

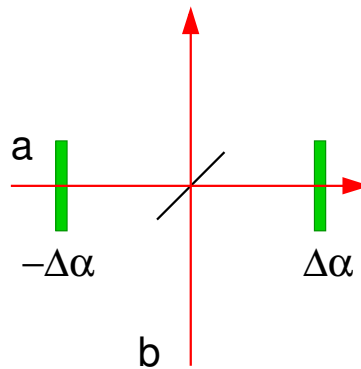


Figure 3.4: Phase shift compensation in the case where the phase shifts occur only in the reflected beams

$\Delta\alpha = (2n + 1)\pi$ and $t_H^2 = t_V^2 = 0.5$ it is $|\psi^+\rangle$ which always splits up while all other Bell states don't, so that $|\psi^+\rangle$ can be detected with just one detector in every output beam. In all other cases every Bell state splits up with a certain probability meaning that no perfect detection of a particular Bell state is possible. Especially for $\Delta\alpha = (2n + 1)\frac{\pi}{2}$ every Bell state splits up with a probability of about $\frac{1}{2}$. The beamsplitter we used for the Bell state analysis had the transmissivities $t_H^2 = t_V^2 = 0.52$, which allows almost perfect performance as shown in Fig. 3.6.

General case

For the sake of completeness it will be checked whether the phase shift compensation is still possible if there are also phase shifts in the transmitted beams. The best one can do is to insert one retarder plate in every input and output mode of the beam splitter as shown in Fig. 3.5.

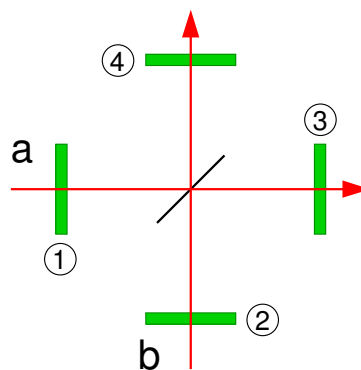
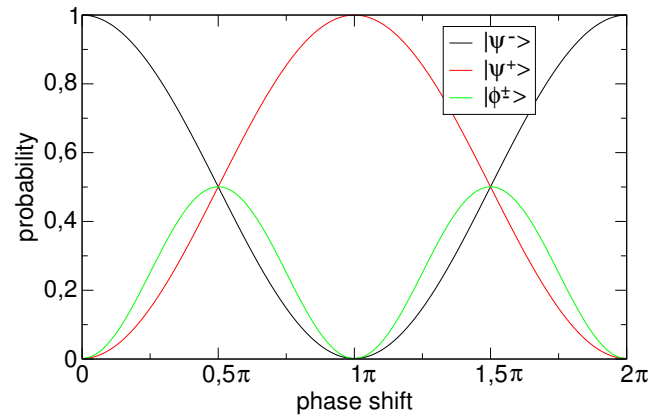
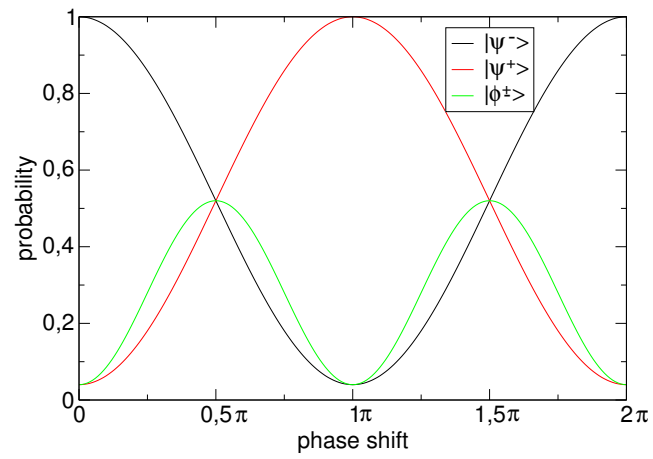


Figure 3.5: All four possibilities of placing retarder plates in order to compensate phase shifts

$$t_H^2 = t_V^2 = 0.52$$



$$t_H^2 = t_V^2 = 0.60$$



$$t_H^2 = 0.45$$

$$t_V^2 = 0.55$$

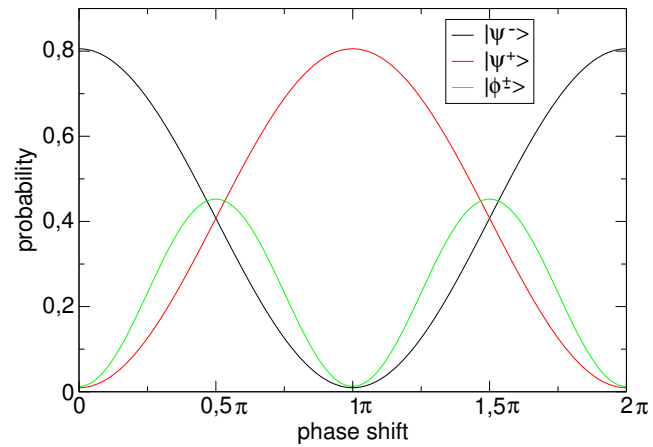


Figure 3.6: Probability for two photons to split up at a beamsplitter for each of the four Bell states as two-photon input states, as function of the phase shift of the beam splitter

The complete transformation is then

$$\underline{B}' = \underline{C}_4 \underline{C}_3 \underline{B} \underline{C}_2 \underline{C}_1$$

with

$$\underline{C}_{1/3} = \begin{pmatrix} e^{i\phi_{1/3}} & 0 & 0 & 0 \\ 0 & 1 & 0 & 0 \\ 0 & 0 & 1 & 0 \\ 0 & 0 & 0 & 1 \end{pmatrix} \quad \underline{C}_{2/4} = \begin{pmatrix} 1 & 0 & 0 & 0 \\ 0 & e^{i\phi_{2/4}} & 0 & 0 \\ 0 & 0 & 1 & 0 \\ 0 & 0 & 0 & 1 \end{pmatrix},$$

resulting in

$$\underline{B}' = \begin{pmatrix} t_H e^{i(\beta_{Ha} + \phi_1 + \phi_3)} & r_H e^{i(\alpha_{Hb} + \phi_2 + \phi_3)} & 0 & 0 \\ r_H e^{i(\alpha_{Ha} + \phi_1 + \phi_4)} & t_H e^{i(\beta_b + \phi_2 + \phi_4)} & 0 & 0 \\ 0 & 0 & t_V e^{i\beta_{Va}} & r_V e^{i\alpha_{Vb}} \\ 0 & 0 & r_V e^{i\alpha_{Va}} & t_V e^{i\beta_{Vb}} \end{pmatrix}.$$

The phase shifts ϕ_1, \dots, ϕ_4 of the retarder plates must be chosen in such a way that for every path through the beamsplitter the phase factors for H and V are the same. This leads to the following conditions

$$\begin{aligned} \phi_1 &= \alpha_{Va} - \alpha_{Ha} - \phi_4 \\ \phi_2 &= \beta_{Vb} - \beta_{Hb} - \phi_4 \\ \phi_3 &= \alpha_{Ha} - \alpha_{Va} + \beta_{Va} - \beta_{Ha} + \phi_4 \\ &= -\alpha_{Hb} + \alpha_{Vb} - \beta_{Vb} + \beta_{Hb} + \phi_4, \end{aligned}$$

which can always be fulfilled with just three plates since ϕ_4 can be chosen arbitrarily and therefore every possible phase shift of a beamsplitter can be compensated.

3.2.2 Hong Ou Mandel dip

For interference to occur at the Bell state analyser the two photons must not contain any information about their origin after being overlapped at the beam splitter, i.e. it must be impossible to detect which photon entered the beam splitter in which input mode. Such information might be given by different arrival times, spectra or spatial modes. The Hong Ou Mandel dip [16] is a two photon interference effect which is helpful to align the Bell state analyser in such a way that this distinguishing information is minimized.

Let two otherwise indistinguishable photons enter a beamsplitter in the input modes a and b . They can be described by the photon number state

$$|\psi_{in}\rangle = |1\rangle_a |1\rangle_b.$$

Then the state on the output side of the beam splitter is

$$|\psi_{out}\rangle = (t^2 - r^2)|1\rangle_a |1\rangle_b + i\sqrt{2}rt|2\rangle_a |0\rangle_b + i\sqrt{2}rt|0\rangle_a |2\rangle_b.$$

The first term vanishes in case of a 50:50 splitting ratio. This means that both photons will always leave the beam splitter in the same output mode and therefore no coincidences should be registered between two detectors in the output modes.

Interference between two down conversion photons

The two-photon input state of the beam splitter $|\psi_{in}\rangle$ could be realised by a photon pair of a first order down-conversion emission, the source being aligned in a way to emit $|\phi^+\rangle$. Then the Fock state above is obtained if just one polarisation component, for example H, is selected by the use of polarisers. But in practice the down-converted photons are never monochromatic, the two-photon state can rather be represented by the linear superposition

$$|\psi_{in}\rangle = \int d\omega_a \int d\omega_b f_a(\omega_a) f_b(\omega_b) \delta(\omega_{P_0} - \omega_a - \omega_b) |1\rangle_a |1\rangle_b,$$

where ω_{P_0} is the frequency of the pump beam and $f_a(\omega_a)$ and $f_b(\omega_b)$ are some weight functions which are peaked at $\omega_a = \omega_b = \frac{\omega_{P_0}}{2}$.

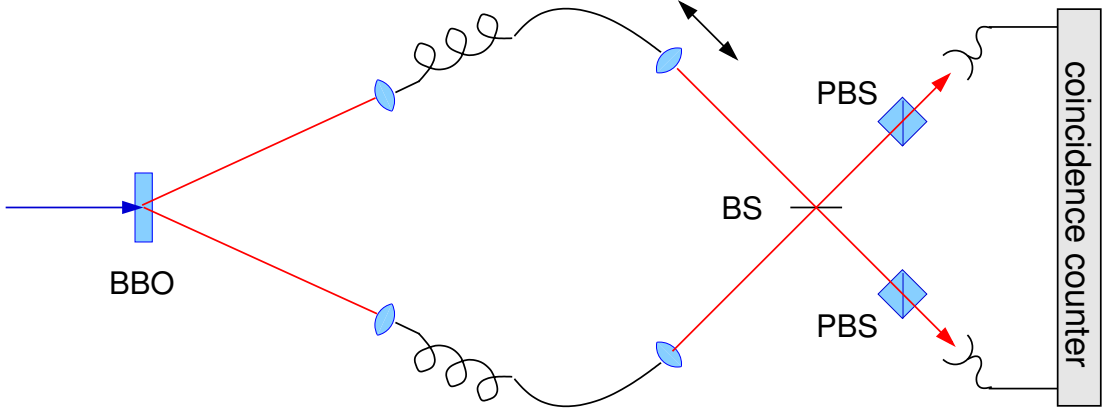


Figure 3.7: Setup for the measurement of the Hong Ou Mandel dip

Maximal interference occurs only if both photons arrive at the beam splitter at exactly the same time. The time delay $\delta\tau$ can be varied by changing the path length of one of the photons; in the setup shown in Fig. 3.7 this can be done by moving one of the fiber couplers as indicated by the black arrow. If the spectral distributions f_a and f_b of the input state are Gaussian in $\omega_{a,b}$ with bandwidth $\Delta\omega$

$$f_{a,b}(\omega_{a,b}) \sim \exp\left[-2\frac{(\omega_{a,b} - \frac{\omega_{P_0}}{2})^2}{\Delta\omega^2}\right],$$

the number N_c of observed photon coincidences versus time delay $\delta\tau$ is given by [16]

$$N_c = C(r^4 + t^4) \left[1 - \frac{2r^2 t^2}{r^4 + t^4} e^{-\frac{1}{8}(\Delta\omega\delta\tau)^2}\right],$$

where C is the photon pair count rate. For $r = t = \frac{1}{\sqrt{2}}$ this reduces to

$$N_c = \frac{C}{2} [1 - e^{-\frac{1}{8}(\Delta\omega\delta\tau)^2}]. \quad (3.8)$$

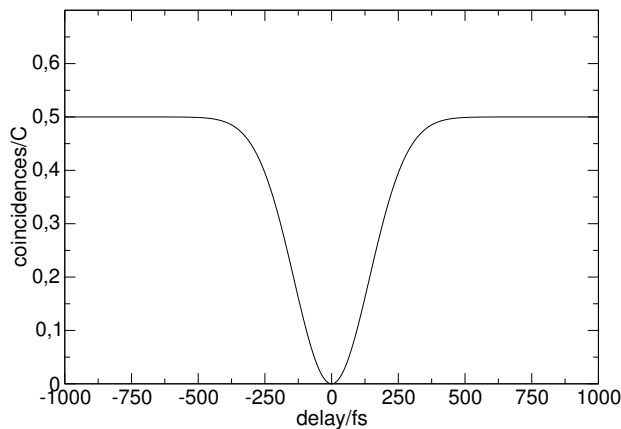


Figure 3.8: The HOM dip

In Fig. (3.8) N_c ist plotted against $\delta\tau$ for $\Delta\omega = 10^{13}\frac{1}{s}$. This dip of the coincidence count rate at zero delay can be used to align the temporal overlap of the two photons. Imperfections of the alignment of the spatial overlap, a splitting ratio other than 50:50, different spectra of the two photons or accidental coincidences can cause a non-vanishing coincidence count rate at zero delay. All those influences determine the **visibility** V of the dip which can be included in Eq. (3.8) like

$$N_c = \tilde{C} [1 - V e^{-\frac{1}{8}(\Delta\omega\delta\tau)^2}] \quad (3.9)$$

and thus provides a measurement of the quality of the overlap.

Interference between a down conversion photon and a weak coherent state

For the experiment we used a weak coherent state as input state to be teleported or telecloned. Since this state had to be projected onto the Bell state basis together with a down conversion photon, interference between those two states has to be studied. For simplicity both states are approximated by single photon states here, effects of higher order contributions are studied in the experimental chapter.

A coherent state is given by the following superposition of photon number states.

$$|\alpha\rangle = e^{-\frac{1}{2}|\alpha|^2} \sum_{n=0}^{\infty} \frac{\alpha^n}{\sqrt{n!}} |n\rangle$$

The probabilities for zero, one or two photons in the state are

$$\begin{aligned} p_0 &= e^{-|\alpha|^2} && \approx 1 - |\alpha|^2 \\ p_1 &= e^{-|\alpha|^2} |\alpha|^2 && \approx |\alpha|^2 \\ p_2 &= \frac{1}{2} e^{-|\alpha|^2} |\alpha|^4 && \approx \frac{1}{2} |\alpha|^4 \end{aligned}$$

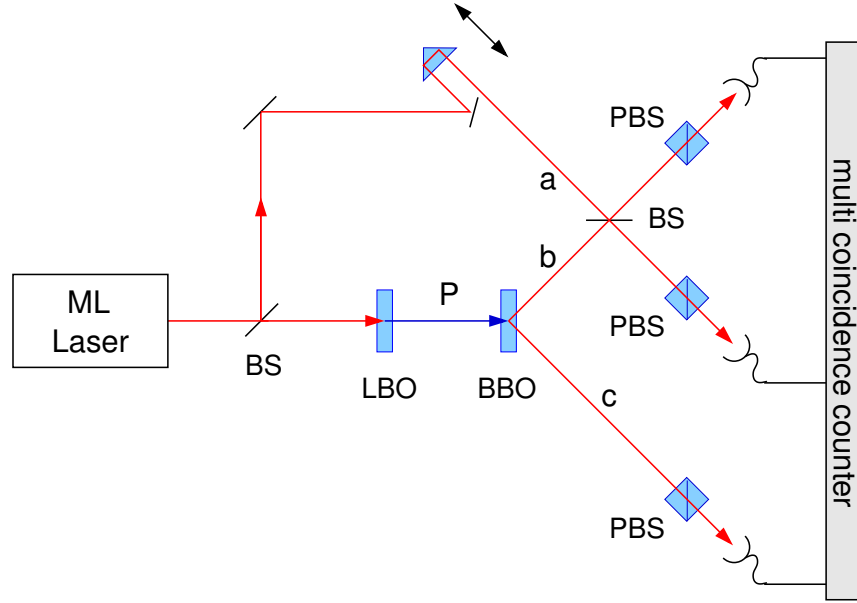


Figure 3.9: Setup for the overlap of a down conversion photon and a weak coherent state and the mean photon number is given by

$$\langle \alpha | \hat{n} | \alpha \rangle = \langle \alpha | a^\dagger a | \alpha \rangle = |\alpha|^2.$$

A coherent state can be realised by a laser beam with a frequency spectrum $f_a(\omega_a)$. If the intensity is very low ($|\alpha|^2 \ll 1$), it can be written as

$$|\psi\rangle_a \approx \sqrt{1 - |\alpha|^2} |0\rangle + \alpha \int d\omega_a f_a(\omega_a) |1\rangle.$$

At low pump power the state emitted by the down conversion source, if again only one polarisation mode is selected, can be approximated by

$$|\psi\rangle_{bc} \approx \sqrt{1 - |c|^2} |0\rangle + \frac{c}{2} \int d\omega_P d\omega_b d\omega_c f_P(\omega_P) f_b(\omega_b) f_c(\omega_c) \delta(\omega_P - \omega_b - \omega_c) |1\rangle_b |1\rangle_c.$$

where ω_P is the frequency of the pump beam and $\omega_{b,c}$ are the frequencies of the down converted photons emitted into the spatial modes b and c .

$|\psi\rangle_{bc}$ can be used to approximate a one photon state in mode b by using the partner photon in mode c as a trigger, i.e. the detection of a photon in mode c gates the detection of a photon in mode b . This state in mode b is overlapped with the weak coherent state in mode a at the beam splitter. To synchronise the arrival of both photons the attenuated laser beam is taken from the same mode locked laser as is used to pump the down conversion after frequency doubling, see Fig. 3.9. Again the path length of one of the input photons is made variable, for example by a movable prism as indicated by the arrow in Fig. 3.9.

The frequency spectra of the different beams can be selected by interference filters. In the case of Gaussian filter functions

$$f_P(\omega_P) \sim \exp \left[-2 \frac{(\omega_P - \omega_{P_0})^2}{\Delta\omega_P^2} \right] \quad \text{and} \quad f_{a,b}(\omega) \sim \exp \left[-2 \frac{(\omega - \frac{\omega_{P_0}}{2})^2}{\Delta\omega^2} \right]$$

the coincidence count rate for two detectors in the output modes of the beam splitter as function of the time delay $\delta\tau$ is given by [17]

$$N_c = C \left[1 - \frac{2r^2t^2}{r^4 + t^4} \tilde{V} \exp \left[- \left(\frac{\delta\tau^2 \Delta\omega^2}{8(1 + \frac{\Delta\omega^2}{2\Delta\omega_P^2})} \right) \right] \right] \quad \text{with} \quad \tilde{V} = \sqrt{\frac{1}{1 + \frac{\Delta\omega^2}{2\Delta\omega_P^2}}}, \quad (3.10)$$

where r^2 and t^2 are the reflectivity and the transmissivity of the beam splitter. Compared to the HOM dip of two down conversion photons (Eq. 3.2.2), the visibility of this dip is reduced by the factor \tilde{V} which is unity for $\Delta\omega \ll \Delta\omega_P$ and falls as $\Delta\omega$ increases. For $\Delta\omega > \Delta\omega_P$ it falls rapidly, corresponding to the fact that the photons are in principle distinguishable if the time uncertainty due to the spectral filtering ($\sim \Delta\omega^{-1}$) is smaller than the pulse duration ($\sim \Delta\omega_P^{-1}$). In this case also the width of the dip grows.

3.3 Measurement of density matrices

The state of a quantum system can be estimated on the basis of a sequence of measurements done on a large enough number of identically prepared copies of the quantum system [29]. In the method of tomographic reconstruction the density matrix of the system is linearly related to a set of measured quantities. Subsequent most likelihood estimation ensures the measured density matrices to represent physical states. The procedure is presented for the measurement of polarisation states of photons.

Single photon state tomography

The Pauli matrices form a basis of the two dimensional Hilbert space. Therefore any density matrix of a qubit, for example the polarisation state of a photon, can be written as a linear combination

$$\rho = a_0\sigma_0 + \vec{a}\vec{\sigma}. \quad (3.11)$$

The coefficients a_0, \dots, a_3 can be determined by four projection measurements given by the four operators

$$\begin{aligned} \mu_0 &= |H\rangle\langle H| & \mu_1 &= |V\rangle\langle V| \\ \mu_2 &= |+\rangle\langle +| & \mu_3 &= |R\rangle\langle R|. \end{aligned}$$

Note that this is just one example of infinitely many possible sets of operators. The expectation values for the number of detected photons are given by $n_i = N_i \text{tr}(\rho\mu_i)$, where N_i is the number of photons which would be detected without polarisation analysis,

depending on the light intensity, detector efficiency and measurement time. Thus the coefficients are obtained in the following way

$$\begin{aligned}
 a_0 &= \frac{1}{2}(\langle H|\rho|H\rangle + \langle V|\rho|V\rangle) = \frac{1}{2} \\
 a_x &= \langle +|\rho|+\rangle - a_0 = \frac{n_2}{N_2} - \frac{1}{2} \\
 a_y &= a_0 - \langle R|\rho|R\rangle = \frac{1}{2} - \frac{n_3}{N_3} \\
 a_z &= \langle H|\rho|H\rangle - a_0 = \frac{n_0}{N_0} + \frac{1}{2},
 \end{aligned}$$

with the first equation including the normalisation property of density matrices, $tr(\rho) = 1$. For the examination of the copy states obtained in the teleportation and telecloning experiments, we were mainly interested in their fidelity with respect to the input state $|\psi_{in}\rangle$, which is given by

$$F = \langle \psi_{in} | \rho_{copy} | \psi_{in} \rangle$$

and can be obtained by a projection measurement corresponding to the operators

$$|\psi_{in}\rangle\langle\psi_{in}| \quad \text{and} \quad |\psi_{in}^\perp\rangle\langle\psi_{in}^\perp|.$$

Multiple photon state tomography

The method described above can be generalised for the measurement of density matrices of two or more photons. The state of an n-qubit system may be written as

$$\rho = \frac{1}{2^n} \sum_{i_1, i_2, \dots, i_n=0}^3 r_{i_1, i_2, \dots, i_n} \sigma_{i_1} \otimes \sigma_{i_2} \otimes \dots \otimes \sigma_{i_n}$$

Analogous to the single photon case, the coefficients r_{i_1, i_2, \dots, i_n} can be related to the outcomes of projection measurements represented by the 4^n operators

$$\mu_{i_1} \otimes \mu_{i_2} \otimes \dots \otimes \mu_{i_n} \quad \text{with} \quad i_k = 0, 1, 2, 3 \quad \text{and} \quad k = 1, 2, \dots, n$$

A tomographically complete set of measurements for the case of a two-photon state and the corresponding calculation of the entries of the density matrix can be found in [29].

Maximum likelihood estimation

The density matrices obtained by quantum state tomography are, by construction, normalised. But due to experimental noise they might fail to be Hermitian and positive semidefinite, and therefore don't correspond to a physical state. This problem can be solved by the application of the maximum likelihood estimation, in which the physical density matrix being most likely to produce the experimental data is found by numerical

optimisation.

The idea is to define a matrix ρ_p as a function of 4^n real parameters t_1, \dots, t_{4^n} in such a way, that it is always representing a physical density matrix of an n qubit system, and a likelihood function as the probability for ρ_p to produce the measured data set dependent on the parameters t_1, \dots, t_{4^n} . The maximum of this function yields the optimal estimate of the measured density matrix. In [29] this function is calculated for the case of a two qubit system.

4 Experiment

This chapter describes the experimental procedures and results. In Section 4.1 an overview of the complete experimental setup is given, and some parts of it are studied in more detail. As described in section 3.1, the four-photon entangled state used for the implementation of quantum telecloning was obtained directly from parametric down conversion. A characterisation of the source, in form of a measurement of the countrate and the visibility of the correlations of the two- and four-photon states, is presented. It follows a description of the preparation of the weak coherent state, which carried the polarisation state to be telecloned.

The interference of the weak coherent state and one of the down conversion photons, which was necessary for the Bell state analysis, strongly depends on the spectra of the different beams and the pulse duration, as shown in section 3.2.2. Therefore the laser pulses were characterised by a measurement of their duration and spectrum, and the transmittance of the spectral filters has been checked. Finally it is described how the five-photon state was analysed.

Section 4.2 deals with the stepwise alignment of the overlap of two beams at a beam splitter for the Bell state analysis. We started with strong laser light, since it offered the possibility of observing interference effects with a CCD camera or even with the naked eye. The transition to quantum interference was done by measuring the Hong Ou Mandel dip between two down conversion photons, since in this case it was much easier to find the temporal overlap and the coincidence count rates were much higher as for the interference of a weak coherent state and a down conversion photon, which followed in the last step.

Finally the experimental results obtained for quantum teleportation and quantum telecloning are presented in sections 4.3 and 4.4. The measured fidelities of the output states to the input states are shown, and for the telecloning also a measurement of the density matrices of the clones.

4.1 The setup

Fig. 4.1 shows the complete experimental setup. The same laser is used to pump the down conversion source after frequency doubling and to provide the weak coherent beam after strong attenuation. The two beams from down conversion are coupled into single mode fibers and directed into two separate analysers, where they are split up at beam splitters. In analyser 1 one of the output beams of the beam splitter is mixed with the

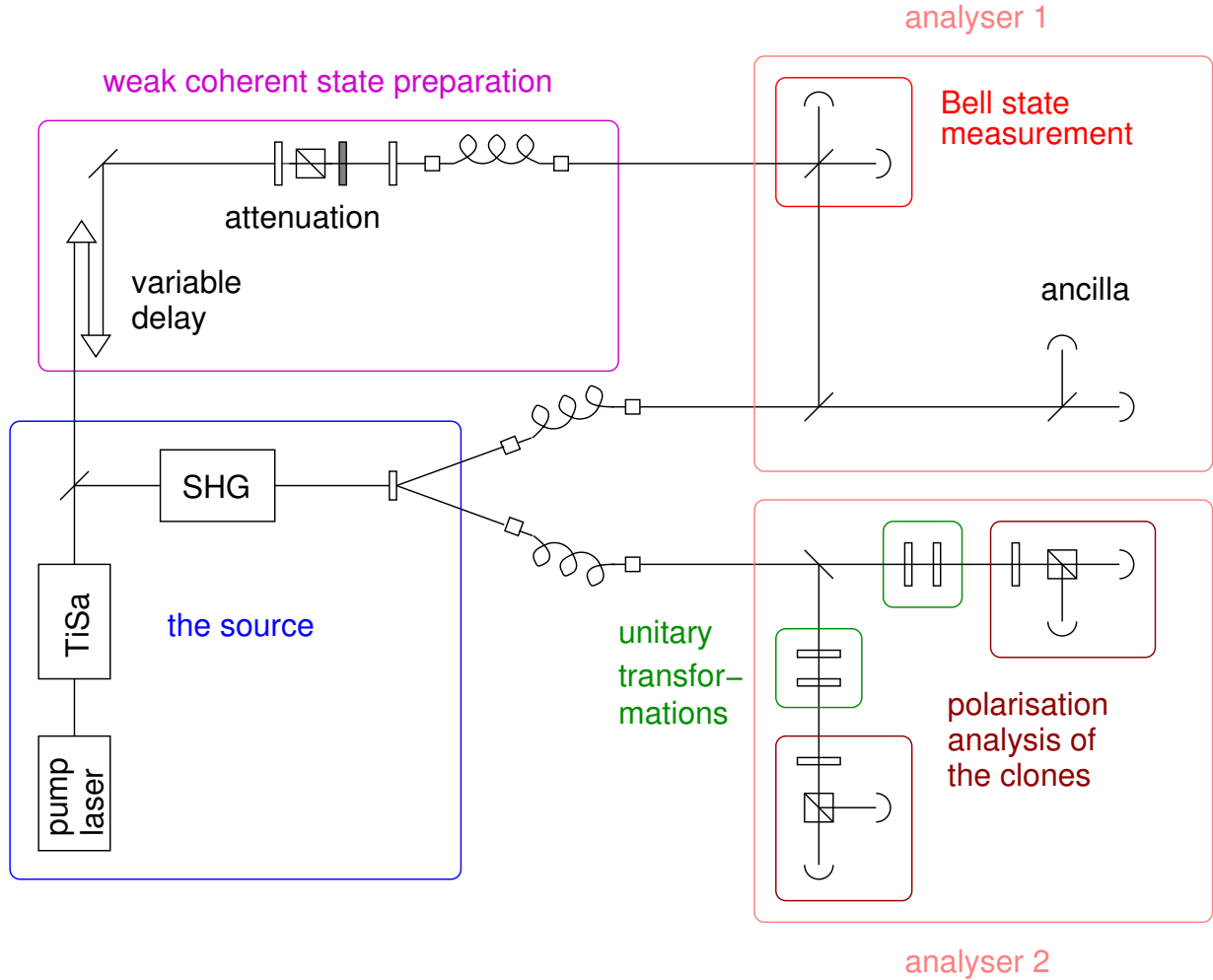


Figure 4.1: The experimental setup

weak coherent beam at a beam splitter for the Bell state analysis. In analyser 2 the unitary transformation and polarisation analysis of the cloned states is performed. The different parts of the setup are described in detail in the next sections.

4.1.1 The source of entangled photons

The photon source is sketched in Fig. 4.2. The laser used for the experiment is a mode locked femtosecond Ti:Sa (titan sapphire) laser operating at $\lambda = 780nm$ with a repetition rate of 82 MHz. It is pumped by a frequency doubled diode pumped cw Nd:YVO₄ (neodymium yttrium vanadate) laser at $\lambda = 532nm$. The pulsed red light is focused on a LBO crystal to obtain the second harmonic at $\lambda = 390nm$ (UV-light), which is again focused on a BBO crystal where it is down converted to single photons at $\lambda = 780nm$. The wavelength, spectral width and pulse length of the Ti:Sa laser can be tuned by aligning

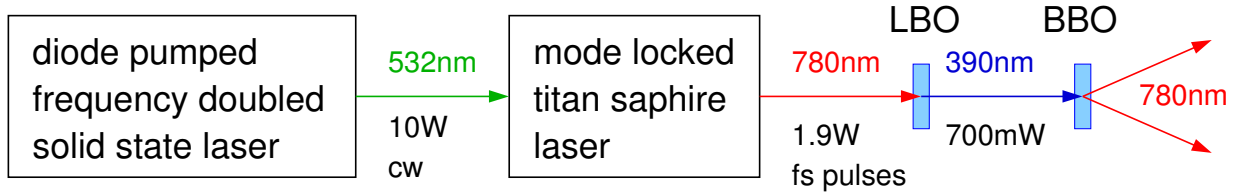


Figure 4.2: The source of entangled photons

a prism pair and a slit in the cavity, the pulses always being near transform limited. A characterisation of the laser pulses and the down conversion source is given below.

Measurement of the pulse length by autocorrelation

To determine the duration of femtosecond laser pulses, a measurement device with a response time smaller than the pulse length is needed. Since response times realisable with semiconductor electronics are in the order of nanoseconds, the measurement can't be done just with a photodiode and an oscilloscope. But the pulse can easily be scanned by itself by the use of autocorrelation.

The principle of an autocorrelator is shown in Fig. 4.3. The laser pulse is split in two by

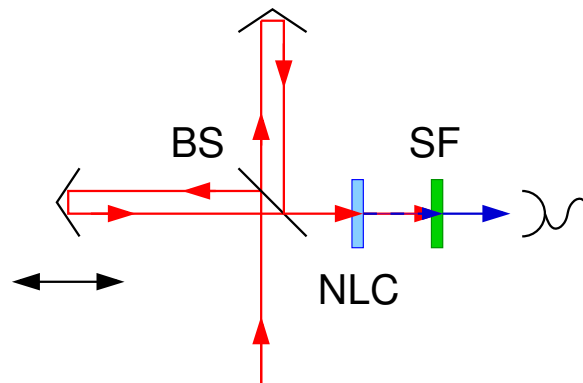


Figure 4.3: Principle of an autocorrelator

a beamsplitter. In each output mode is a mirror reflecting the replica back to the beam splitter where they are overlapped. By moving one of the mirrors the path length for one beam can be varied, hence changing the temporal overlap of the two pulses. In case of **field autocorrelation** the intensity of the superposed beams is measured by a photo diode with an output signal proportional to the intensity of the incident light. The detection signal $G(\tau)$ is proportional to [27]

$$G(\tau) \propto \int_{-\infty}^{\infty} dt |E(t) + E(t - \tau)|^2 = G_E(0) + G_E(\tau),$$

where $E(t)$ is the electric field strength of the pulse, τ is the time delay caused by the path length difference $\Delta l = c\tau$ and

$$G_E(\tau) = \int_{-\infty}^{\infty} dt(E(t)E^*(t-\tau) + E^*(t)E(t-\tau)) = \frac{1}{\pi} \int_{-\infty}^{\infty} d\omega |\tilde{E}(\omega)|^2 e^{i\omega\tau}$$

is the field autocorrelation function with $\tilde{E}(\omega)$ being the fourier transform of $E(t)$. Since $G_E(\tau)$ is just the fourier transform of the intensity spectrum, $G(\tau)$ gives no more information than the spectrum itself.

More information, for example about the phase of the pulse, can be gained by **interferometric autocorrelation** where the detection signal is proportional to the intensity squared.

$$G(\tau) \propto \int_{-\infty}^{\infty} dt |E(t) + E(t-\tau)|^4$$

This can be realised by detecting the second harmonic of the initial signal, by the use of a nonlinear crystal in the output beam and subsequent spectral filtering as shown in Fig. 4.3, or, as in the case of our autocorrelator, by using a photodiode which is sensitive only to two photon processes. The autocorrelation curve can be recorded directly by moving the mirror periodically and displaying Δl and the detection signal on an oszilloscope in the xy -mode. The x axis can be calibrated as time axis by utilizing the fact that the distance between two maxima of $G(\Delta l)$ is $\frac{\lambda}{2} = c\frac{T}{2}$. The width of this curve $\Delta\tilde{\tau}$ is proportional to the pulse width $\Delta\tau$

$$\Delta\tau = \frac{\Delta\tilde{\tau}}{f},$$

with the factor f depending on the pulse shape. Most femtosecond lasers generate $sech^2$ pulses where $f = 1.543$ [26]. In this case the product of the spectral width $\Delta\nu$ and pulse width, the time-bandwidth product, is

$$\Delta\tau\Delta\nu \geq 0.3148.$$

Pulses reaching this lower bound are called **transform limited**. Fig. 4.4 shows two different combinations of pulse width and spectral width of the Ti:Sa laser beam. Note that $\Delta\lambda$ and $\Delta\tau$ are stated as FWHM. With

$$\Delta\nu = \frac{c}{\lambda_0^2} \Delta\lambda,$$

the corresponding time-bandwidth products are 0.4099 and 0.4035, respectively.

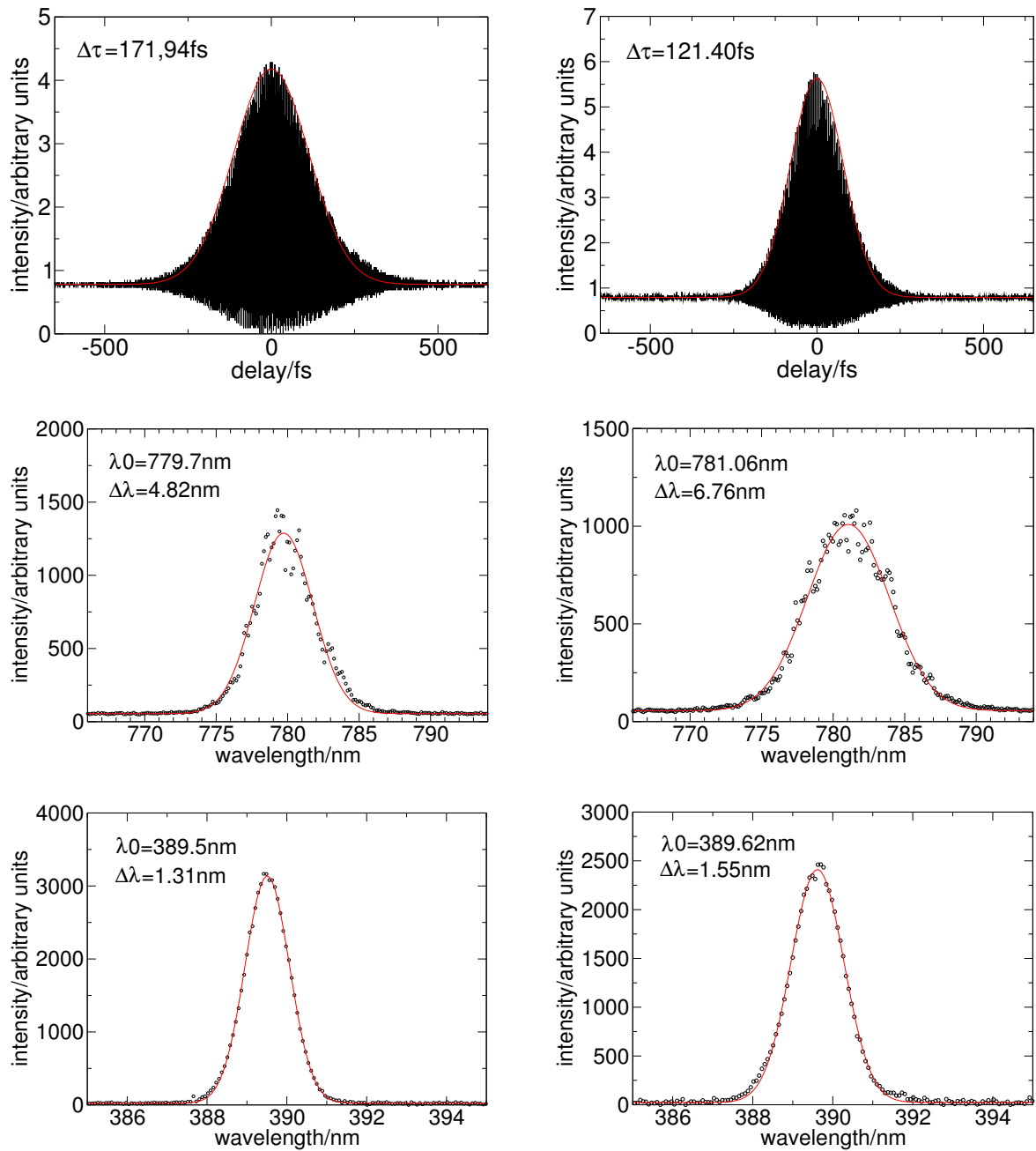


Figure 4.4: Two different combinations of pulse width, spectrum of the red light of the Ti:Sa laser and spectrum of the UV light obtained by the second harmonic generation, corresponding to two different laser alignments

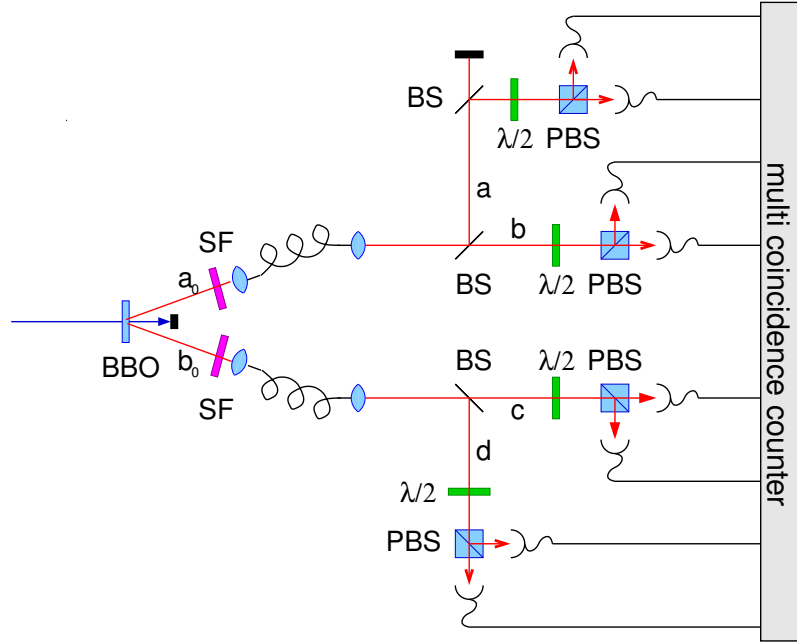


Figure 4.5: Setup for the measurement of the 2- and 4-photon correlations

Characterisation of the down conversion source

The quality of the down conversion alignment can be measured by the visibility of the correlations in the different bases. This can be determined by a projection of the photons in all four spatial modes ($x = a, b, c, d$ as shown in Fig. 4.5) onto two orthogonal states [9]

$$|l_x, \phi_x\rangle = \frac{1}{\sqrt{2}}(|R\rangle_x + l_x e^{i\phi_x} |L\rangle_x) \quad \text{with } l_x = \pm 1,$$

where for example $\phi_x = 0$ or $\phi_x = \frac{\pi}{2}$ correspond to an analysis in the HV-basis or 45° -basis, respectively.

For the **two-photon correlation function** of the photon pairs coming from first order down conversion emission, it is sufficient to consider only two spatial modes, for example b and c . The theoretical correlation function is then given by the expectation value of the product of the polarisation observables $|l_b, \phi_b\rangle\langle l_b, \phi_b|$ and $|l_c, \phi_c\rangle\langle l_c, \phi_c|$. The experimental function can be obtained from the four two-fold coincidence count rates c_{l_b, l_c} like

$$E(\phi_b, \phi_c) = \frac{\sum_{l_b, l_c} l_b l_c c_{l_b, l_c}}{\sum_{l'_b, l'_c} c_{l'_b, l'_c}}.$$

The visibility of the correlations in a particular measurement basis is given by the maximum of this function for one analyser angle fixed defining the measurement basis.

The **four-photon correlation function** is obtained in an analogous manner from the 16

four-fold coincidences c_{l_a, l_b, l_c, l_d}

$$E(\phi_a, \phi_b, \phi_c, \phi_d) = \frac{\sum_{l_a, l_b, l_c, l_d} l_a l_b l_c l_d c_{l_a, l_b, l_c, l_d}}{\sum_{l'_a, l'_b, l'_c, l'_d} c_{l'_a, l'_b, l'_c, l'_d}}.$$

The dependence of this function on the angle ϕ_b with all other analysers fixed at $\phi_a = \phi_c = \phi_d = 0$ has been shown for our down conversion source in [9]. The visibility is again given by the maximum of the correlation function. For the down conversion emission given by Eq. 3.1 on Page 21, maximal correlations are obtained for all analyser angles being the same. Figs. 4.6 and 4.7 show correlation measurements in the HV-basis and the 45° -basis. Since the detectors exhibit different efficiencies, the count rates have been corrected for their relative efficiencies. The twofold coincidences have been measured between the four detectors

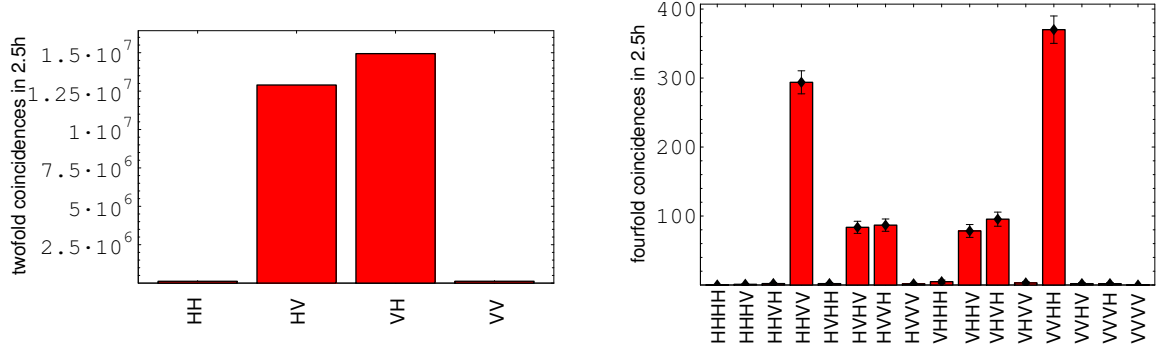


Figure 4.6: Measurement of the 2- and 4-photon correlations in the HV-basis

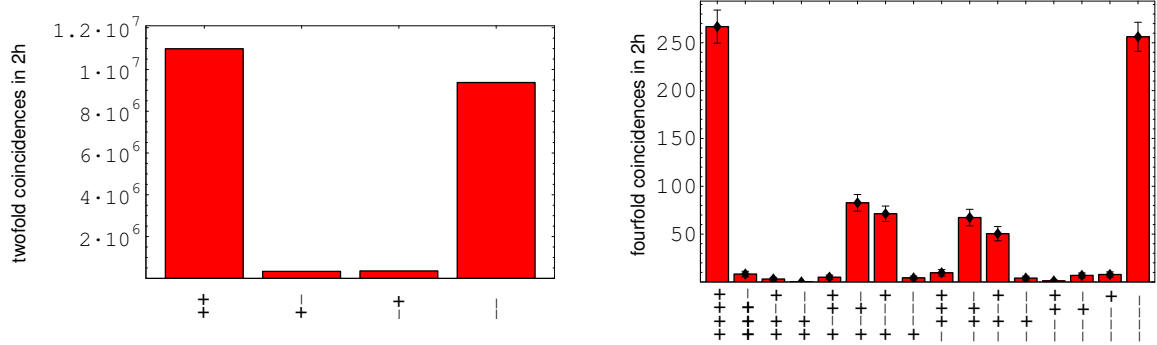


Figure 4.7: Measurement of the 2- and 4-photon correlations in the 45° -basis

in modes b and c , with a count rate of about $3000 \frac{1}{s}$. Therefore the overall two-photon count rate in all four spatial modes is about $12000 \frac{1}{s}$. The count rate for the fourfold coincidences was about $0.125 \frac{1}{s}$, which has to be doubled because we used only one output mode of the overlap beamsplitter in analyser 1 (see Fig. 4.5) for this measurement, giving 0.25 4-photon states per second. The visibilities were $V_{HV} = 98.3\%$ and $V_{45} = 93.5\%$ for the 2-photon correlations and $V_{HV} = 96.4\% \pm 3.1\%$ and $V_{45} = 88.4\% \pm 3.5\%$ for the 4-photon correlations.

4.1.2 Weak coherent state preparation

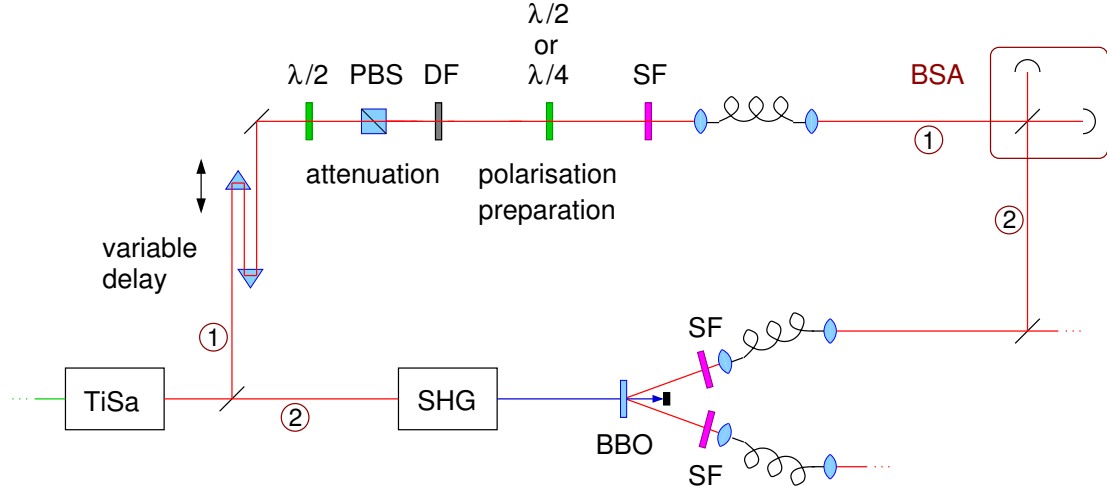


Figure 4.8: Preparation of the weak coherent state

As input state for both teleportation and telecloning we used a weak coherent state, realised by an attenuated laser beam. As shown in Fig. 4.1 and 4.8 we just picked off a small fraction of the red laser light. This has the advantage that the pulses are synchronised with the down conversion emissions and that this beam has the same central wavelength of 780nm. But for a weak coherent state there is always the possibility of getting more than one photon per pulse. Together with the high probability of losing down conversion photons, this causes the occurrence of unwanted events which can't be distinguished from the proper events appearing in the schemes of teleportation and telecloning as presented in the sections 2.4 and 2.6. The problem of such background events will be explained in more detail in section 4.2.3.

The preparation of the weak coherent state includes the adjustment of the path length, of the attenuation and of the polarisation. In order to get the temporal overlap of the photons of the weak coherent state and the down conversion photons the lengths of path 1 and 2, as shown in Fig 4.8, have to be made equal. Therefore path length 2 was measured with a ruler and path length 1 was adapted roughly with an optical delay unit formed by two prisms. One of the prisms was mounted on a translation stage driven by a motor for a precise adjustment of the path length which was achieved by searching the Hong Ou Mandel dip of a heralded down conversion photon and the weak coherent state (see section 4.2.3).

The attenuation down to single photon level was done by means of density filters combined with a variable attenuation, realised by a PBS preceded by a half wave plate. By turning the half wave plate the polarisation of the linearly polarised beam can be rotated in such a way that the transmissivity of the PBS varies between 0 and 1. The mean photon number

per pulse $|\alpha|^2$ can be measured with the relation

$$|\alpha|^2 = \frac{1}{R} \left(\frac{S_1}{\eta_1} + \frac{S_2}{\eta_2} \right)$$

where $S_{1/2}$ are the photon count rates per second at the detectors at the Bell state analyser which have the efficiencies $\eta_{1/2}$, and R is the repetition rate of the laser.

The polarisation of the weak coherent beam can be aligned by the use of either a half or a quarter wave plate behind the PBS and the spectral selection is done by a spectral filter identical to the ones used for the down conversion photons. Figs. 4.9 and 4.10 show the spectra of the down conversion photons and the weak coherent beam as measured directly behind the filters.

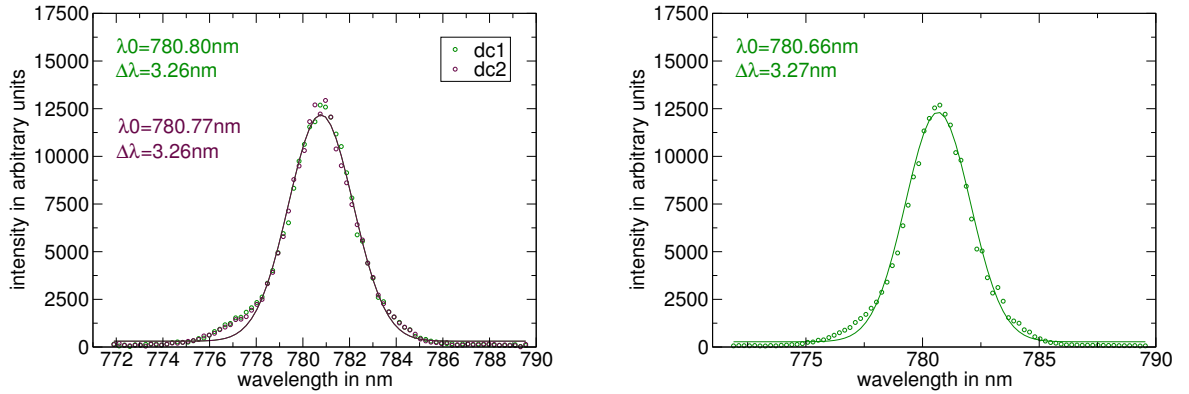


Figure 4.9: Spectra behind the filters in the two down conversion beams

Figure 4.10: Spectrum behind the filter in the weak coherent beam

4.1.3 The analysers

In analyser 2 (Fig. 4.12) two clones of the input state shall be created. The two photons coming from the four-photon down conversion emission are split up at a beam splitter (the cases where they don't split up are discarded by the postselection of the detection events), where a quartz plate compensates the phase shift in the reflected beam. The separated photons pass through a half wave plate at 0° and a half wave plate at 45° . This corresponds to the unitary transformation $\sigma_x \sigma_z$ which transforms the photons into two optimal clones, if ψ^- is detected in the Bell state analyser as shown in section 2.6. The polarisation analysis of the clones is done by a polarising beam splitter, preceded by either a half or a quarter wave plate. In this way the projection onto any orthogonal polarisation basis can be performed. For example any wave plate on 0° constitutes a projection onto the HV-basis, a half wave plate at 22.5° a projection onto the 45° -basis and a quarter wave plate at 45° a projection onto the LR-basis.

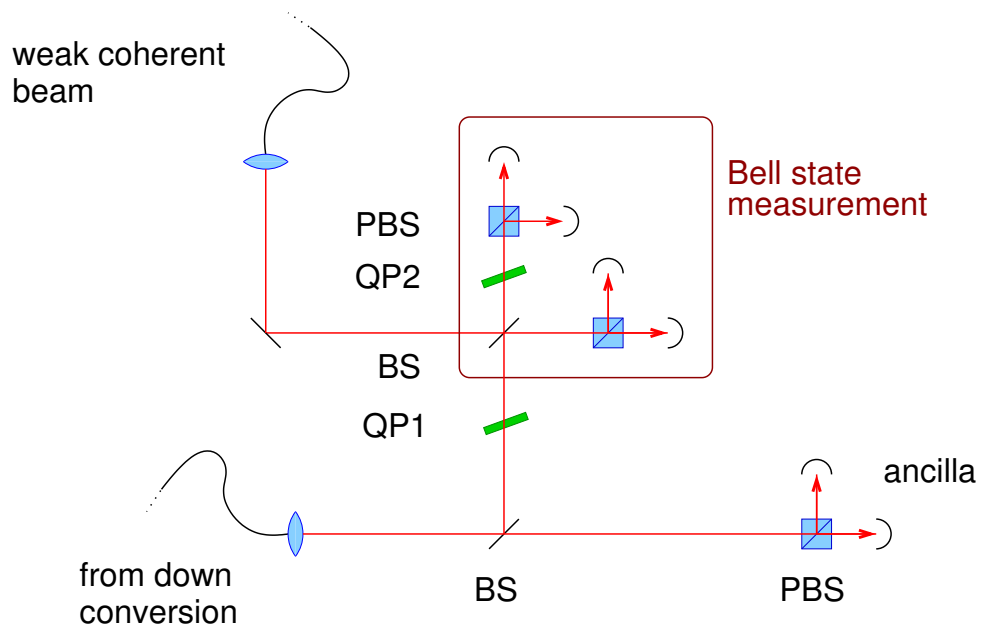


Figure 4.11: Analyser 1

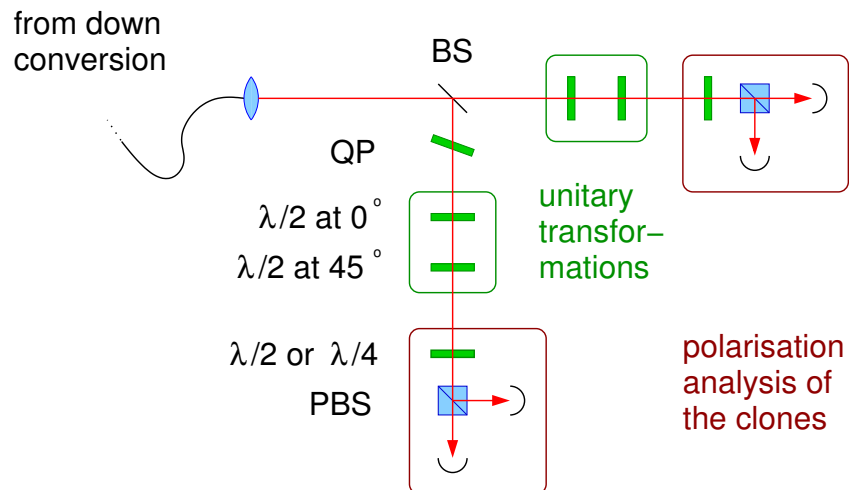


Figure 4.12: Analyser 2

In analyser 1 (Fig. 4.11) three photons are detected, two photons from down conversion and one photon derived from the weak coherent beam representing the input state. The down conversion photons are again split up at a beam splitter. One of them is just detected as ancilla photon, which is necessary for the postselection of events. Without detecting it, one would not know whether the photons really split up at the beam splitter. The second photon is overlapped with the input state at the Bell state analyser. The alignment of this overlap will be described in section 4.2. The phase shift compensation could be implemented with two quartz plates as described in section 3.2.1. In this case the quartz plate QP1 compensates the joint phase shift of both beam splitters.

Due to the low losses of the optical components used in the setup and to the variable focussing provided by a movable lens used for the outcoupling of the fibers, an overall coupling efficiency from single mode fiber to the multimode fiber of the detectors of about 95% could be achieved in both analysers. The detection was done with passive quenched fiber pigtailed Si-avalanche photo diodes (APDs) connected to a multi coincidence unit allowing the registration of all $2^8 = 256$ possible coincidences between 8 detectors at once. This unit was specially designed for the detection of four or five photon states [24]. Since it was not possible to process the signals of more than 8 detectors, two of the ten detectors shown in Fig. 4.12 and 4.11 had to be discarded. The identification of $|\psi^-\rangle$ can be done with just two detectors in the Bell state analyser, therefore the other two detectors and the polarising beam splitters were removed for the telecloning experiment. For the teleportation which was done with the two-photon states from first order down conversion, the two detectors in the ancilla arm were of no use and could be removed. In this case the Bell state analysis was done with all four detectors.

4.2 The overlap

A crucial part of the experiment was the alignment of the overlap between one photon of the 4-photon entangled state emitted by the down-conversion source and the weak coherent state at a beam splitter, in order to perform the Bell state analysis. This has been accomplished in a stepwise process, starting with the interference of visible cw laser light to find the spatial overlap, then switching to pulsed laser light for the temporal overlap. The next step was the transition to quantum interference by aligning the Hong Ou Mandel dip (see section 3.2.2) between two down conversion photons. Finally the weak coherent state was overlapped with a photon from first order down conversion.

4.2.1 Classical interference

As first step the spatial overlap was aligned with the light of a laser diode at $\lambda = 785\text{nm}$. The light was coupled into a single mode fiber beam splitter whose output modes were crossed at the beam splitter as shown in Fig. 4.13. One of the fiber outcouplers was mounted on two translation stages to have the possibility of varying its position in both directions orthogonal to the output beam. Additionally the position of the outcoupling

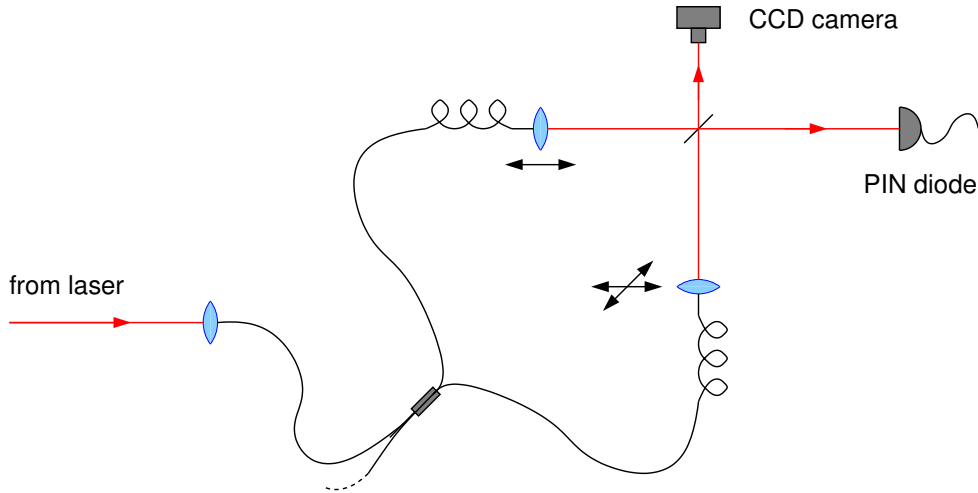


Figure 4.13: Setup for the alignment of the overlap

lense could be changed so that the output angle as well as the focussing could be optimised. The quality of the alignment was checked with a CCD camera in one of the output modes. The goal was to achieve the same position and shape for both beams at two camera positions separated by approximately $2m$. A successful alignment results in a blinking image of the beam cross section, since fluctuations in the phase shifts of the two beams cause alternating constructive and destructive interference, whereas a bad alignment gives rise to interference fringes. Fig. 4.14 shows an example of such an image taken with the CCD camera. With the spatial modes being well aligned the temporal overlap could be searched, i.e. the path lengths for both beams in the analyser were made equal. Therefore the pulsed light of the titan sapphire laser was coupled into the fiber beam splitter. The second output coupler was mounted on a translation stage with which the position in beam direction and thus the path length could be varied. This stage had a motor driven by a computer program which simultaneously registered the voltage at a PIN diode in the output beam of the beam splitter. The plot of this voltage against the motor position exhibits interference fringes with a gaussian envelope, which are maximal for zero delay of the two pulses. Such a measurement is shown in Fig. 4.15. The fit gives a maximal voltage of $7.526V$ and a minimal voltage of $0.186V$, resulting in a visibility of $V=95.2\%$.

4.2.2 Interference between two down conversion photons

The next step for the alignment of the overlap was the change to single photon level, i.e. the Hong Ou Mandel dip between two down conversion photons was measured. The measurement was carried out exactly as described in section 3.2.2 on page 28 with the setup shown in Fig. 3.7. The detection was now done with two APDs in the output modes of the beam splitter and the coincidences between them were detected with the multi coincidence unit and recorded as function of the path length difference.

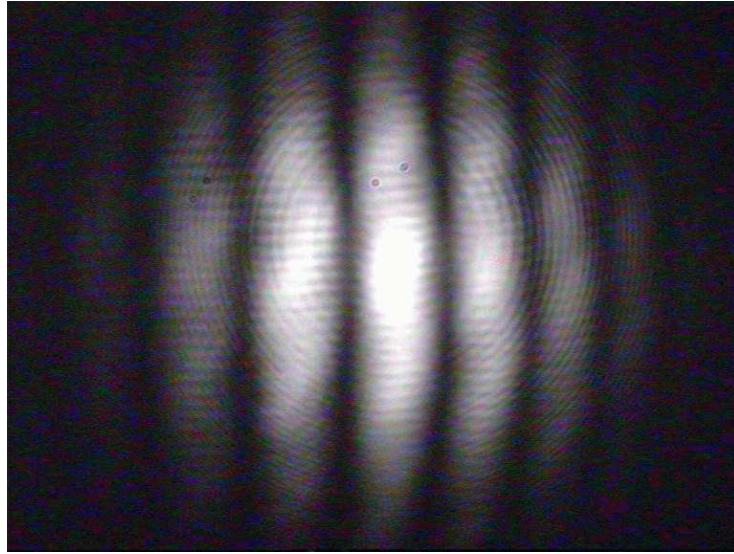


Figure 4.14: Cross section of the overlapping beams, recorded with a CCD camera in the output mode of the beam splitter. In this example the horizontal overlap is not well aligned.

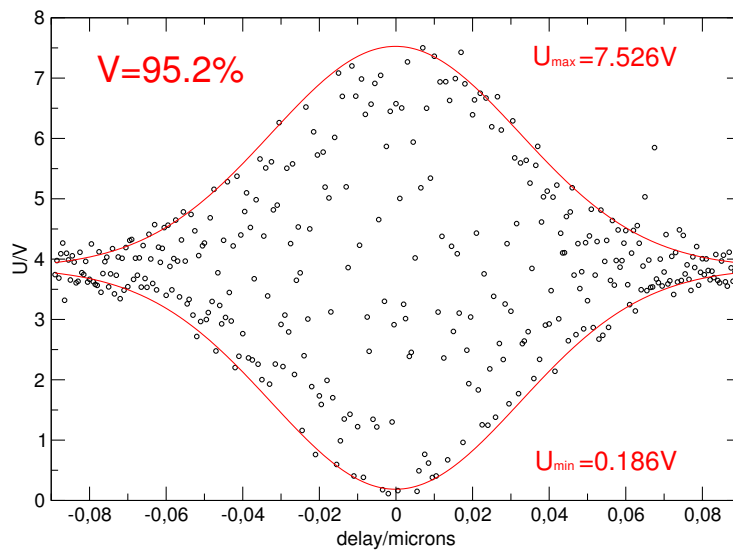


Figure 4.15: Intensity of the overlapping beams against the path length difference (pulsed laser as light source), measured by the voltage of a PIN diode in the output of the beam splitter.

Typically we achieved a visibility of about $V=90\%$ as shown in Fig. 4.16. The

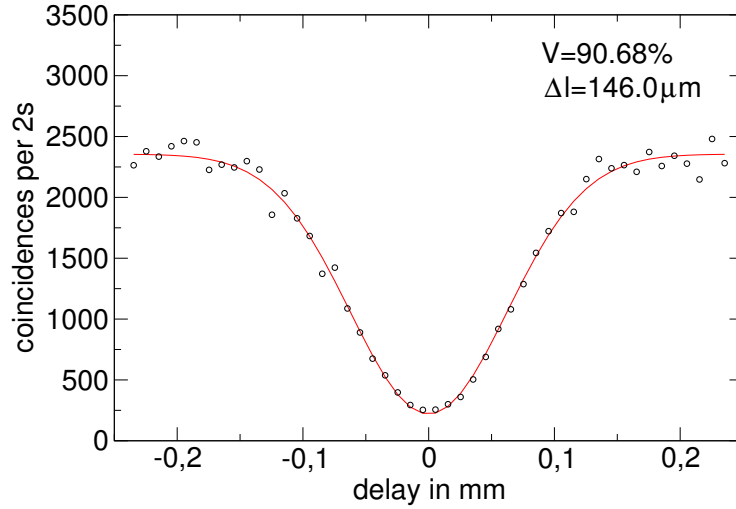


Figure 4.16: Hong Ou Mandel dip between two down conversion photons

theoretical visibility of 100% is reduced if the two photons are distinguishable in some way, by their polarisations, spectra, arrival times or spatial modes (behind the BS) or if the beam splitter has a splitting ratio other than 50:50. The polarisation of the photons was aligned with the polarisation controllers of the fibers and were selected with PBSs with a transmissivity for V of about 0.1%. Their spectra were made identical by the interference filters as shown in Fig. 4.9 and at the minimum of the dip the time delay of the two photons is zero. The transmissivity of the beamsplitter was $t^2 = 52\%$ which reduces the visibility just by a factor of 0.997. So the only reason for a loss of visibility being left was a non-perfect spatial overlap. We could increase the visibility to 94,22% (see Fig. 4.17) by coupling the output beams into single mode fibers and connecting those to the multimode fibers of the detectors, but this caused a dramatic loss of count rate, the coincidence count rate outside the dip was reduced by a factor of 10, and therefore this possibility was not taken into account for the final setup.

The width of the dip provides a measure of the length of the photon wave packet. The FWHM is found to be $\Delta l = 146.0\mu m$ and $\Delta l = 149.5\mu m$ respectively, corresponding to a time of about $\Delta t = 490fs$. The theoretical value can be calculated from Eq. 3.9 on Page 30 as

$$\Delta t = \frac{4}{\Delta\omega} \sqrt{2 \ln 2} = \frac{4 \ln 2}{\pi c} \frac{\lambda^2}{\Delta\lambda},$$

where $\Delta\lambda$ is given as FWHM. The spectral filters used in the down conversion beams transmit a central wavelength of $\lambda = 780.80nm$ with a width of $\Delta\lambda = 3.26nm$ (see Fig. 4.9 on page 43), therefore a coherence time of $\Delta t = 550fs$ would have been expected.

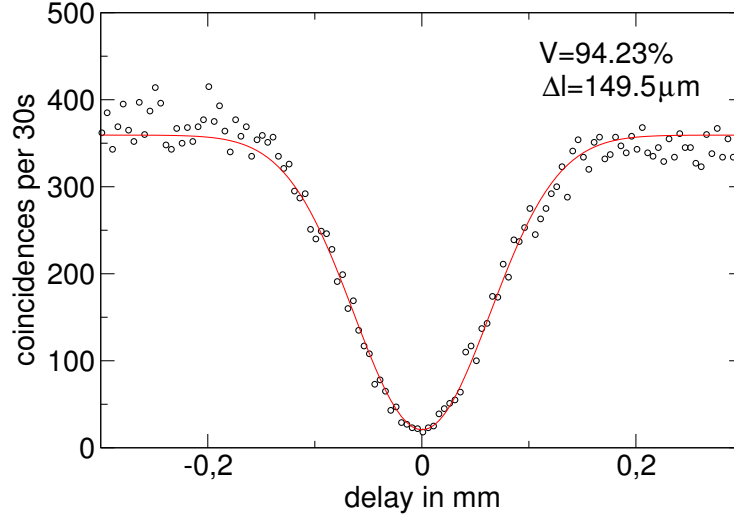


Figure 4.17: Hong Ou Mandel dip between two down conversion photons with the output modes of the beam splitter selected by single mode fibers

4.2.3 Interference between a down conversion photon and a weak coherent state

The overlap of a down conversion photon with a photon of a weak coherent state brings about new difficulties. Although they originate from the same laser source, their appearance is completely independent, i.e. there is no correlation between the emission of a down conversion photon and a photon in the weak coherent beam for each pulse. This lowers the coincidence count rate to a level where unwanted contributions of higher order down conversion emission and of multi-photon emissions in the weak coherent beam become important.

Fig. 4.18 shows the setup we used for the measurement of the dip. As described in section 3.2.2, one photon of a down conversion pair has been overlapped at a beam splitter with the weak coherent state, while its partner was used for the time gating, therefore threefold coincidences have been measured.

The complete state in front of the beam splitters is given by the product $|\alpha\rangle_w |\psi_{DC}\rangle_{a_0 b_0}$ of the weak coherent beam in mode w

$$\begin{aligned}
 |\alpha\rangle_w &= e^{-\frac{1}{2}|\alpha|^2} \sum_{n=0}^{\infty} \frac{\alpha^n}{\sqrt{n!}} |n\rangle_w \\
 &\approx \sqrt{1-|\alpha|^2} |0\rangle_w + \alpha |1\rangle_w + \frac{1}{\sqrt{2}} \alpha^2 |2\rangle_w + \dots
 \end{aligned}$$

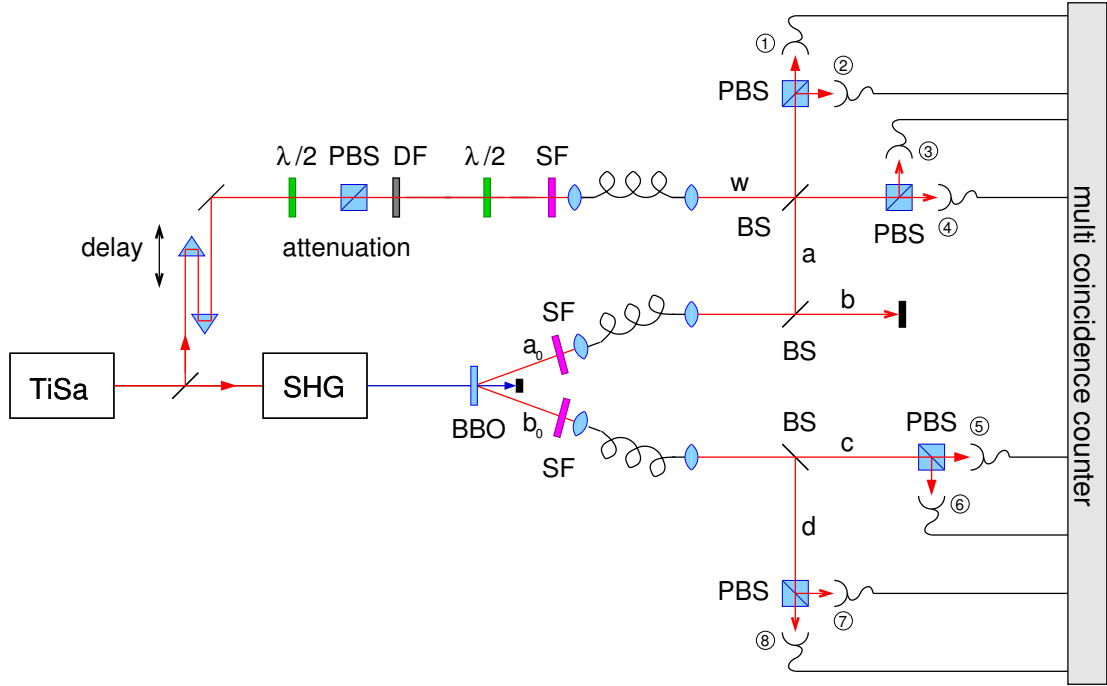


Figure 4.18: Setup for the measurement of the interference between a weak coherent state and a down conversion photon

and the following down conversion emission in modes a_0 and b_0 .

$$\begin{aligned}
 |\psi_{DC}\rangle &= Z \exp[-ic(a_{0H}^\dagger b_{0V}^\dagger - a_{0V}^\dagger b_{0H}^\dagger)]|0\rangle \\
 &\approx |0\rangle - ic(a_{0H}^\dagger b_{0V}^\dagger - a_{0V}^\dagger b_{0H}^\dagger)|0\rangle - \frac{c^2}{2}(a_{0H}^\dagger b_{0V}^\dagger - a_{0V}^\dagger b_{0H}^\dagger)^2|0\rangle + \dots
 \end{aligned}
 \tag{4.1}$$

In case of a horizontally polarised coherent beam only those down conversion pair emissions were selected, where a horizontally polarised photon is emitted into mode a , since for a maximal visibility of the dip of the coincidence count rate the overlapping photons have to be indistinguishable. With the photon pairs from down conversion being in the state $|\psi^-\rangle$, the trigger photon in mode c or d has vertical polarisation. Therefore only threefold coincidences between detectors 1,4,6 and 1,4,7 were recorded. But those detection events can also be caused by other emissions. The two main contributions to such background coincidences originate from second order down conversion emissions and from two-photon emissions in the weak coherent beam.

The four-photon down conversion emissions term $a_{0H}^{\dagger 2} b_{0V}^{\dagger 2}|0\rangle$ leads to background coincidences if both horizontally polarised photons in mode a_{0H} are reflected into mode a and split up at the beam splitter in the Bell state analyser, thus leading to a coincidence at detectors 1 and 4. The third click at detector 6 or 7 can be caused by the corresponding two photons with vertical polarisation in mode b_0 if both are detected by the same detector (which gives the same signal for the detection of one or several photons), or if one of them

gets lost.

Two-photon emissions in the weak coherent beam combined with the emission of a vertically polarised down conversion photon in mode b_0 constitute another contribution of background triple coincidences. The appendant horizontally polarised down conversion photon in mode a_0 can either get lost (which is most probable) or be detected at detectors 1 or 4 or be transmitted into mode b where no detection is possible.

The factor c in Eq. (4.1) as well as the collection efficiency of the down conversion photons can be determined experimentally from the singles and coincidence count rates of the down conversion emission [33]. With those values the probabilities of the different background events can be calculated and compared with the probability of the coincidences of interest, i.e. their ratio can be determined. Very detailed calculations in this vein have been performed by Sascha Gaertner and will be presented in his PhD thesis.

Experimentally this ratio could be determined by measuring the threefold coincidence count rate with modes w and a blocked one after the other and comparing it with the overall count rate outside the dip (without the temporal overlap). All threefold coincidence detections with a beam blocker in mode w originate from higher order down conversion emissions while coincidences between detectors 1 and 4 are caused by multi-photon emissions in the weak coherent beam if mode a is blocked.

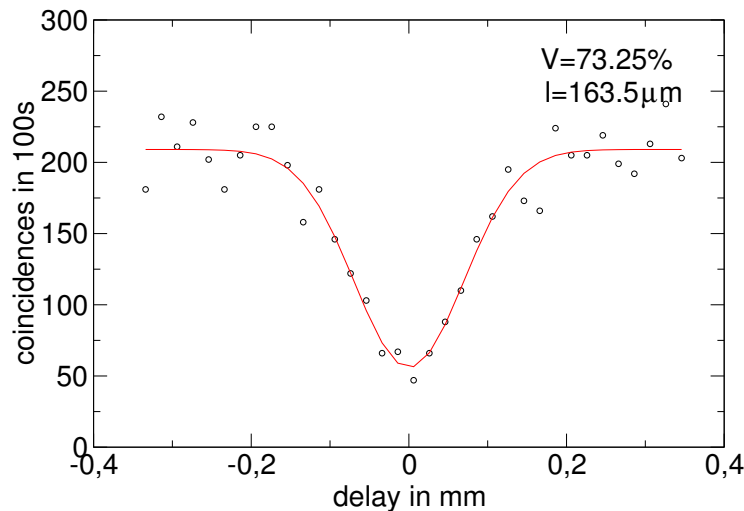


Figure 4.19: Interference between a weak coherent state and a photon from down conversion

Fig. 4.19 shows a dip of the threefold coincidence count rate between detectors 1,4 and 6 with a visibility of $V = 73.3 \pm 3.0\%$, measured with the setup shown in Fig. 4.18. The corresponding background contribution was $b = 13.2\% \pm 1.1\%$. To measure the quality of

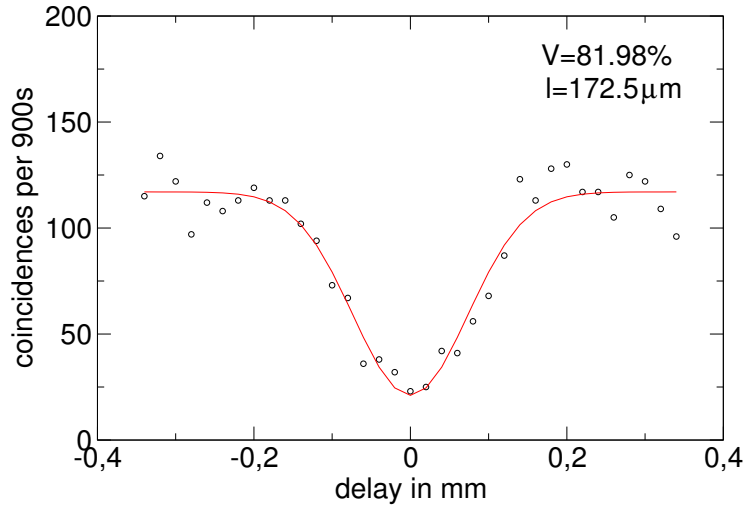


Figure 4.20: Interference between a weak coherent state and a photon from down conversion with both beams being strongly attenuated

the overlap, this background has to be subtracted, which results in the corrected visibility

$$V_{corr} = \frac{(C_{max} - bC_{max}) - (C_{min} - bC_{max})}{C_{max} - bC_{max}} = \frac{V}{1 - b} = 84.4\% \pm 3.6\%,$$

where C_{max} is the count rate outside the dip, C_{min} is the minimal count rate at the bottom of the dip and bC_{max} is the count rate of the background coincidences.

For the HOM dip with a photon pair from down conversion we achieved visibilities of about 90%. The loss of visibility compared to this value can be explained by the additional factor \tilde{V} given in Eq. (3.10) on Page 32. The spectral width of the filters used for all three beams is given by $\Delta\lambda \approx 3.3nm$ (see Figs. 4.9 and 4.10), but the spectral width of the pump beam, which depends on the laser alignment as shown in Fig. 4.4, was not measured at this day, just a typical value of $\Delta\lambda_P = 1.5nm$ can be assumed. In this case the visibility is reduced by the factor

$$\tilde{V} = \sqrt{\frac{1}{1 + \frac{\Delta\omega^2}{2\Delta\omega_P^2}}} = \sqrt{\frac{1}{1 + \frac{\Delta\lambda^2}{32\Delta\lambda_P^2}}} \approx 96.7\%$$

for $\lambda = 2\lambda_P$. The visibility of the dip with the down conversion photons can be used as a measure for the quality of the spatial overlap, giving an additional factor of $V_{sp} = 90\%$. Therefore the visibility of the dip with the weak coherent beam after background subtraction would have been expected to be

$$V_{exp} = \tilde{V}V_{sp} = 86.4\%$$

which lies within the error range of the measured value. By lowering the power of the pump beam of the down conversion source by means of an iris to about 100mW and attenuating the coherent beam even stronger, the background contribution could be reduced to $5.4\% \pm 1.6\%$. At the same time the overall count rate of threefold coincidences outside the dip was reduced from $2.1 \frac{1}{s}$ (see Fig. 4.19) to $0.13 \frac{1}{s}$. In this way the visibility of the dip could be increased to $V = 82.0\% \pm 3.2\%$ (see Fig. 4.20). Background subtraction leads to the corrected value $V_{corr} = 86.7\% \pm 3.7\%$, which is even closer to the expected value calculated above.

4.3 Quantum teleportation

Quantum teleportation was performed with the setup shown in Fig. 4.18. The input state was realised by approximating the ideal of a single photon with a specific polarisation state with the component $|1\rangle$ of the polarised weak coherent state in mode w . The Bell state $|\psi^-\rangle$ was provided by the first order down conversion emission into modes a_0 and b_0 . If the photon in mode a_0 was reflected into mode a , it was projected onto the Bell state basis together with the photon of the weak coherent beam. The Bell state analyser consisted of a beam splitter and two polarising beam splitters in its output modes, allowing the identification of $|\psi^+\rangle$ and $|\psi^-\rangle$. Since we had no possibility to change the unitary transformation of the third photon depending on the outcome of the Bell state measurement, we confined ourselves to the detection of $|\psi^-\rangle$. In this case no unitary transformation is necessary, and therefore the third photon in mode c or d just had to be analysed, i.e. projected onto some polarisation basis by the use of a half or quarter wave plate and a polarising beam splitter. We always chose the eigenbase of the input state for the analysis of the copy state to obtain its fidelity to the input state, as shown in section 3.3.

Figs. 4.21, 4.22, 4.23 and 4.24 show the teleportation of four different input states. Each plot shows threefold coincidences corresponding to the detection of $|\psi^-\rangle_{aw}|\psi_{in}\rangle_c$ and $|\psi^-\rangle_{aw}|\psi_{in}^\perp\rangle_c$ versus the path length difference $c\delta\tau$ implied by the movement of the prism in the coherent beam. Since the detectors exhibit different detection efficiencies, the measured count rates have been corrected for their relative efficiencies.

In case of the input state $|H\rangle$ for example we used the polarising beam splitters in modes c and d without waveplates for the projection of the copy state onto the HV-basis. Threefold coincidences between detectors 1,3,5 and 2,4,5 both represent detections of $|\psi^-\rangle_{aw}|H\rangle_c$ and have been summed up, as well as threefold coincidences between detectors 1,3,6 and 2,4,6 which correspond to the detection of $|\psi^-\rangle_{aw}|V\rangle_c$. In this case the fidelity of the copy state to the input state equals the probability of the detection of H in mode c which is given by

$$F_H = \frac{C_H}{C_H + C_V} \quad \text{at } c\delta\tau = 0,$$

where $C_{H/V}$ is the threefold coincidence countrates with a horizontally/vertically polarised photon in mode c . The same can be done for the copies reflected into mode d . The resulting

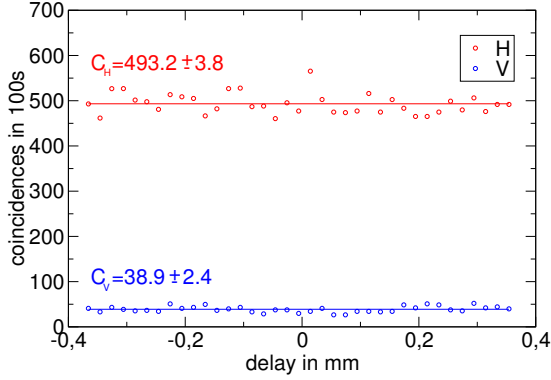


Figure 4.21: Teleportation of $|H\rangle$

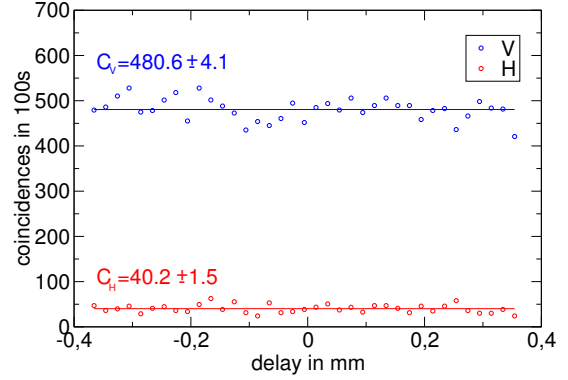


Figure 4.22: Teleportation of $|V\rangle$

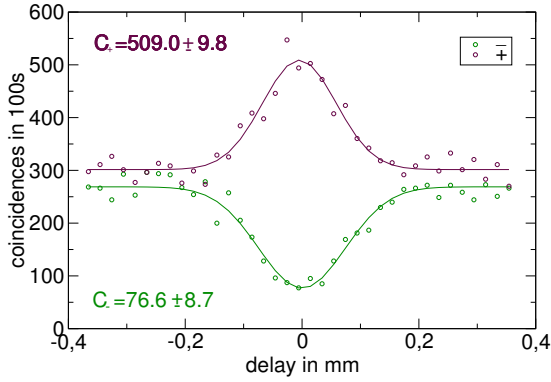


Figure 4.23: Teleportation of $|+\rangle$

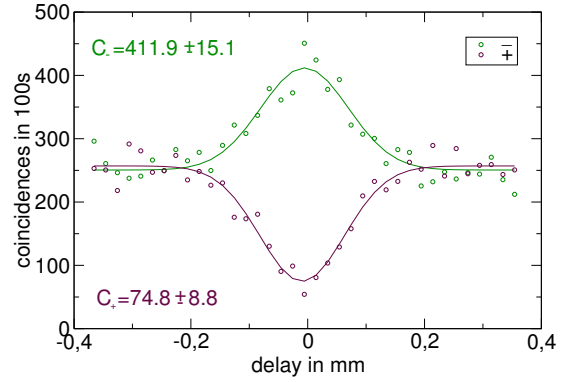


Figure 4.24: Teleportation of $|-\rangle$

fidelties are

$$\begin{aligned}
 F_H &= 92.70\% \pm 0.73\% & F_V &= 92.28\% \pm 0.81\% \\
 F_+ &= 86.92\% \pm 1.73\% & F_- &= 84.63\% \pm 3.15\%.
 \end{aligned}$$

In case of the input states $|H\rangle$ and $|V\rangle$ the fidelity of the copies is independent of the delay time of the two photons entering the Bell state analyser, which means that in those cases no overlap, i.e. no projection onto the Bell state basis is necessary. For example for $|H\rangle$ in mode w and $|\psi^-\rangle$ in modes a and c the detection of a horizontally and a vertically polarised photon in the output modes of the overlap beam splitter always corresponds to the detection of a vertically polarised photon in mode c , independent of any interference effects. However for the input states $|+\rangle$ and $|-\rangle$ the fidelity of the copies without the temporal overlap is 50% and is maximal for zero delay of the overlapping photons.

The higher fidelities for the teleportation of $|H\rangle$ or $|V\rangle$ compared to the teleportation of

$|+\rangle$ and $|-\rangle$ are due to lower background contributions, since in those cases two photon emissions in the weak coherent beam can't cause coincidences between detectors 1 and 3 or 2 and 4. For the teleportation of $|+\rangle$ and $|-\rangle$ the background contribution has been determined experimentally (again by blocking beam w and beam a one after the other) as $b_{+/-} = 16.9\% \pm 1.9\%$, where $13.1\% \pm 1.6\%$ come from down conversion emissions and $3.9\% \pm 0.9\%$ are caused by two-photon emissions in the weak coherent beam. Since this background is white noise, which means that it produces every measurement result with the same probability, it can be subtracted from the measured count rates like

$$\begin{aligned} C'_{H/V} &= C_{H/V} - \frac{1}{2}(C_H + C_V)b_{H/V} \\ C'_{+/-} &= C_{+/-} - \frac{1}{2}(C_+ + C_-)b_{+/-}, \end{aligned}$$

and therefore the corrected fidelities can be calculated like

$$F_{corr} = \frac{F - \frac{b}{2}}{1 - b}.$$

For the teleportation of $|+\rangle$ and $|-\rangle$ this results in

$$F_{+,corr} = 94.4\% \quad F_{-,corr} = 91.7\%.$$

The background for the teleportation of $|H\rangle$ and $|V\rangle$ has not been measured but can be assumed to be approximately as high as the part of $b_{+/-}$ originating from down conversion emissions, which gives

$$F_{H,corr} = 99.1\% \quad F_{V,corr} = 98.7\%.$$

The loss of fidelity compared to the theoretical value of 100% can be explained by the non-perfect two-photon correlations, and, in case of the teleportation of $|+\rangle$ and $|-\rangle$, by the non-perfect overlap of the two photons in the Bell state analyser.

4.4 Quantum telecloning

After the quality of the setup has been proven by the successful teleportations, the telecloning could be started. Instead of three-photon events we now had to detect five-photon events including second order down conversion emissions. This brings about the new difficulty of an extremely low count rate. An estimate of the count rate can be obtained as follows.

The measurement of the four-photon correlations (see section 4.1.1) gave a four-photon count rate of $0.25 \frac{1}{s}$, which corresponds to $C_4 = 3 \cdot 10^{-9}$ four-photon events per pulse. The maximal mean photon number of the weak coherent beam detectable with the passively quenched APDs was about 0.012 per pulse. With a detector efficiency of 0.4 this results in a singles count rate of $C_1 = 0.005$ per pulse. Thus a five-photon count rate of $C_5 = C_4 \cdot C_1 = 1.5 \cdot 10^{-11}$ per pulse, corresponding to $0.0012 \frac{1}{s} = 4.4$ per hour would have

been expected. Since we detected just one of the four Bell states and discarded all other detection events, this has to be divided by 4, which results in a count rate of 1.2 events per hour.

During the first measurements we really obtained 1 to 1.5 events per hour. To get the error on the fidelity of the clones below 5%, at least 100 detection events were needed, which requires a measurement time of the order of three days. Since it was very hard work to keep the whole system stable for such a long time, we decided to exchange the two passively quenched APDs in the Bell state analyser by two actively quenched APDs. The dead time of those diodes is reduced by fast electronics accomplishing the quenching and recharging after an avalanche breakdown [34], which leads to a higher efficiency and to possible count rates of up to 10^7 counts per second. Because the multi coincidence unit can process a maximal number of $8 \cdot 10^5$ detection events per second [24] and because all fivefold coincidences of interest included a coincidence between the two detectors in the Bell state analyser (if $|\psi^-\rangle$ is detected), we used an additional two channel coincidence unit to transform coincidences between those detectors into single signals to be sent to the eight channel unit. The new setup is shown in Fig. 4.25.

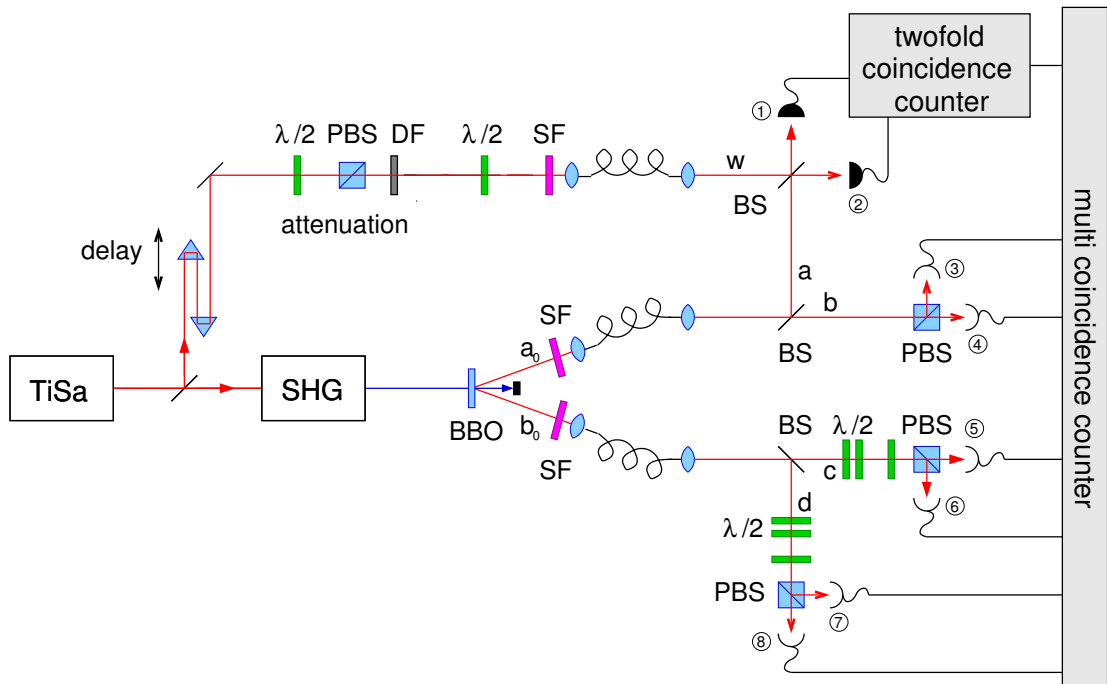


Figure 4.25: Telecloning setup

4.4.1 Telecloning of three different input states

For the telecloning experiment we measured fivefold coincidences between the two detectors in the Bell state analyser (corresponding to the detection of $|\psi^-\rangle$), one detector in mode

b (ancilla photon) and one detector in both arms c and d , where the clones of the input state are analysed.

At first we chose the eigenbase of the input state as analysis basis to obtain the fidelity of the clones. All fivefold detection events including two clicks at the detectors in the Bell state analyser and one click at one of the detectors in the ancilla arm were summed up and the numbers were corrected for the relative efficiencies of the detectors. The count rates of the remaining four different detection events are shown in Figs. 4.26, 4.27 and 4.28 for the input states $|H\rangle$, $|+\rangle$ and $|R\rangle$, where the first letter denotes the polarisation of clone 1 in mode c and the second denotes the polarisation of clone 2 in mode d .

The fidelity of the clones is given by the probability of their polarisation being parallel to the polarisation of the input state. For example for the input state H the fidelity of clone 1 is given by

$$F_1 = \frac{C_{HH} + C_{HV}}{C_{HH} + C_{HV} + C_{VH} + C_{VV}},$$

where C_{HH} is the number of detection events with both clones having horizontal polarisation (first bar in Fig. 4.26), etc. This gives the following fidelities:

input state $ H\rangle$:	$F_1 = 73.3\% \pm 4.7\%$	$F_2 = 69.6\% \pm 4.9\%$
input state $ +\rangle$:	$F_1 = 69.7\% \pm 4.8\%$	$F_2 = 68.0\% \pm 4.9\%$
input state $ R\rangle$:	$F_1 = 70.3\% \pm 4.0\%$	$F_2 = 68.1\% \pm 4.1\%$

All of them are above the classical limit given by 66.67% (see section 2.5.3), even though the error bars reach into the classical regime. The errors include poissonian distribution of the five-photon events as well as errors in determination of the detector efficiencies.

Again the loss of fidelity compared to the theoretical value of 83.33% (see section 2.5.2) is mainly due to background events. In this case third order down conversion emissions are involved, making an estimation of the background much more complex. Those calculations have been carried out by Sascha Gaertner and will be presented in his PhD thesis. For the down conversion intensity corresponding to $c \approx 0.07$ we adjusted the mean photon number in the weak coherent beam to $|\alpha|^2 = 0.03$, since at this working point a minimal background contribution of $b \approx 26\%$ was expected. Smaller background contributions could only have been achieved by attenuating the down conversion source, but this idea was abandoned because it would have led to lower count rates again. The number of measured fivefold events was 90 for the telecloning of $|H\rangle$, 92 for the input state $|+\rangle$ and 135 for the input state $|R\rangle$. The measurement time was 15h in each case, which gives a count rate of 6 to 9 events per hour. This helpful increase can be explained by the efficiency of the actively quenched APDs being $\eta_a = 0.6$ compared to the efficiency $\eta_p = 0.4$ of the passively quenched APDs, which increases the count rate by a factor of $\frac{\eta_a^2}{\eta_p^2} = 2.25$, and an additional factor of 2.5 given by the increase of $|\alpha|^2$ from 0.012 to 0.03. Thus a count rate of $1.2 \cdot 2.5 \cdot 2.25 = 6.75$ events per hour would have been expected. As for the teleportation the corrected fidelities after background subtraction can be calculated like

$$F_{corr} = \frac{F - \frac{b}{2}}{1 - b}.$$

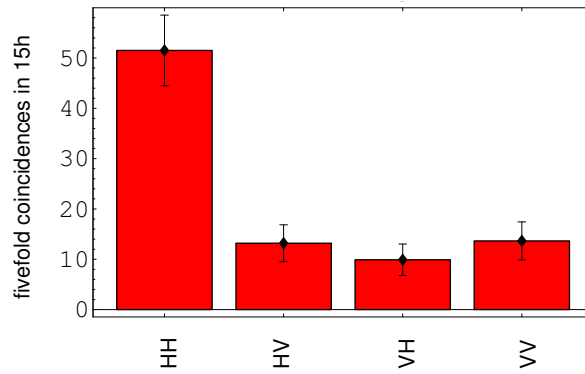


Figure 4.26: Telecloning of $|H\rangle$

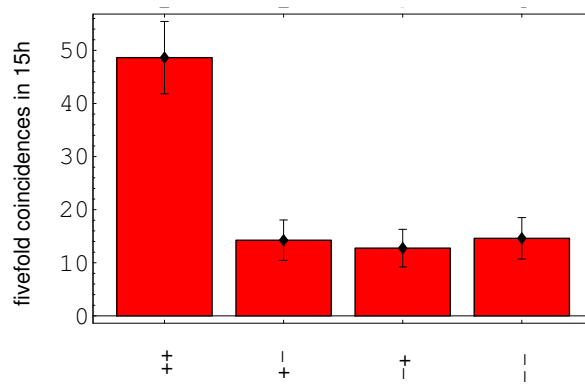


Figure 4.27: Telecloning of $|+\rangle$

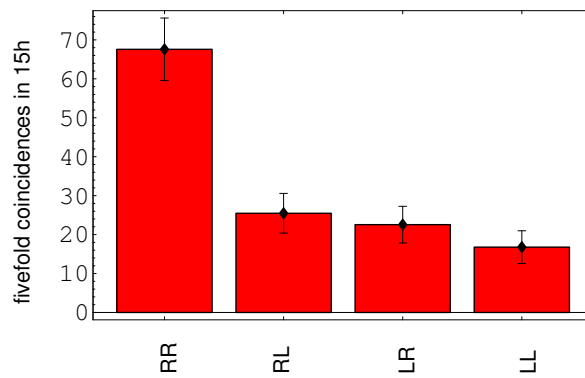


Figure 4.28: Telecloning of $|R\rangle$

With the calculated background contribution $b \approx 26\%$ this results in

$$\begin{array}{lll} \text{input state } |H\rangle : & F_{1,corr} = 81.5\% & F_{2,corr} = 76.5\% \\ \text{input state } |+\rangle : & F_{1,corr} = 76.6\% & F_{2,corr} = 74.3\% \\ \text{input state } |R\rangle : & F_{1,corr} = 77.4\% & F_{2,corr} = 74.5\%. \end{array}$$

Other influences reducing the fidelity of the clones are the non-perfect overlap of the two photons at the Bell state analyser as well as the non-perfect four-photon correlations.

4.4.2 Measurement of the density matrices of the clones

For one input state, namely $|+\rangle$, the states of the clones were examined closer by a measurement of their density matrices. As shown in section 3.3 this can be done by projecting the photon states onto the HV-basis, the 45° -basis and the LR-basis. Using the notation

$$c_H = \frac{C_H}{C_H + C_V} \quad c_+ = \frac{C_+}{C_+ + C_-} \quad c_R = \frac{C_R}{C_R + C_L},$$

where C_H for example is the number of fivefold coincidence detections with the clone being horizontally polarised, the density matrix in the HV-basis can be obtained from the measurement data like

$$\rho_{HV} = \begin{pmatrix} c_H & (c_+ - \frac{1}{2}) - i(\frac{1}{2} - c_R) \\ (c_+ - \frac{1}{2}) + i(\frac{1}{2} - c_R) & 1 - c_H \end{pmatrix},$$

and the density matrix in the 45° -basis is given by

$$\rho_{45} = \begin{pmatrix} c_+ & (c_H - \frac{1}{2}) - i(c_R - \frac{1}{2}) \\ (c_H - \frac{1}{2}) + i(c_R - \frac{1}{2}) & 1 - c_+ \end{pmatrix}.$$

To ensure equal conditions for the measurements in the different bases, the analyser settings have been changed every 15 min. This could be performed by putting a half and a quarter wave plate, each mounted in a rotation stage driven by a motor, in front of the PBSs in modes c and d and controlling the motors by the detection program. An overall count rate of 300 counts in 50h was achieved. The measurement time for the projection onto the 45° -basis was 18.5h, and 15.75h for the other two bases. The following measurement outcomes were obtained:

$$\begin{array}{lll} \text{clone 1 :} & c_H = 0.499 \pm 0.053 & c_+ = 0.723 \pm 0.042 & c_R = 0.561 \pm 0.050 \\ \text{clone 2 :} & c_H = 0.495 \pm 0.054 & c_+ = 0.692 \pm 0.045 & c_R = 0.390 \pm 0.050 \end{array}$$

Therefore the density matrices in the HV-basis are

$$\begin{aligned} \rho_{1,HV} &= \begin{pmatrix} 0.499 & 0.223 - 0.061i \\ 0.223 + 0.061i & 0.501 \end{pmatrix} \pm \begin{pmatrix} 0.053 & 0.043 - 0.050i \\ 0.043 + 0.050i & 0.053 \end{pmatrix} \\ \rho_{2,HV} &= \begin{pmatrix} 0.495 & 0.192 - 0.110i \\ 0.192 + 0.110i & 0.505 \end{pmatrix} \pm \begin{pmatrix} 0.051 & 0.045 - 0.050i \\ 0.045 + 0.050i & 0.051 \end{pmatrix}, \end{aligned}$$

and in the 45° -basis they are given by

$$\begin{aligned}\rho_{1,45} &= \begin{pmatrix} 0.723 & -0.001 + 0.061i \\ -0.001 - 0.061i & 0.277 \end{pmatrix} \pm \begin{pmatrix} 0.043 & 0.053 + 0.050i \\ 0.053 + 0.050i & 0.043 \end{pmatrix} \\ \rho_{2,45} &= \begin{pmatrix} 0.692 & -0.005 - 0.110i \\ -0.005 + 0.110i & 0.308 \end{pmatrix} \pm \begin{pmatrix} 0.045 & 0.051 + 0.050i \\ 0.051 + 0.050i & 0.045 \end{pmatrix}.\end{aligned}$$

As an illustration all matrices are plotted in Figs. 4.29 to 4.32. They have the three important properties of normalisation, Hermiticity and positivity, therefore no maximum likelihood estimation (see section 3.3) is necessary. For the input state $|+\rangle$ the fidelities of the clones are given by c_+ , thus

$$F_1 = 72.33\% \pm 4.25\% \quad F_2 = 69.22\% \pm 4.51\%.$$

Again both fidelities are above the classical limit given by 66.67%. As shown in section 2.6 the theoretical density matrices are given by

$$\rho_{HV} = \begin{pmatrix} 0.5 & 0.333 \\ 0.333 & 0.5 \end{pmatrix} \quad \text{and} \quad \rho_{45} = \begin{pmatrix} 0.833 & 0 \\ 0 & 0.167 \end{pmatrix}.$$

The fidelities of the measured states to the theoretical state are 99.15% for clone 1 and 98.60% for clone 2. This good result is due to the fact that the background events are mainly white noise, which means that they produce every measurement result with the same probability $\frac{1}{2}$. Though this lowers the fidelity to the input state, it doesn't change the measurement results in the HV- and RL-basis where the theory predicts $c_H = c_R = 0.5$.

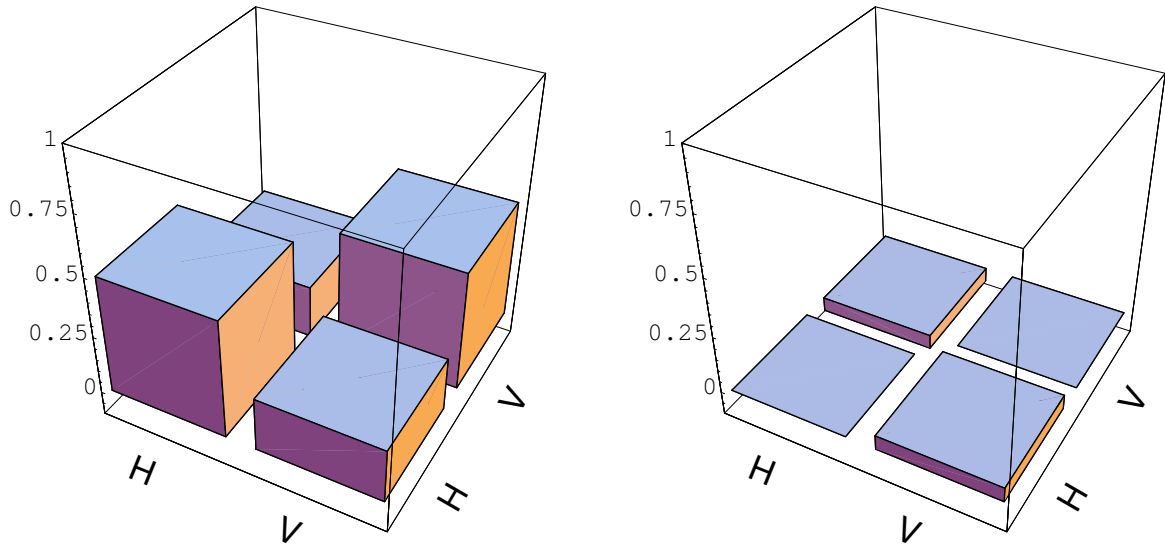


Figure 4.29: Real (left) and imaginary (right) part of the density matrix of clone 1 in the HV-basis

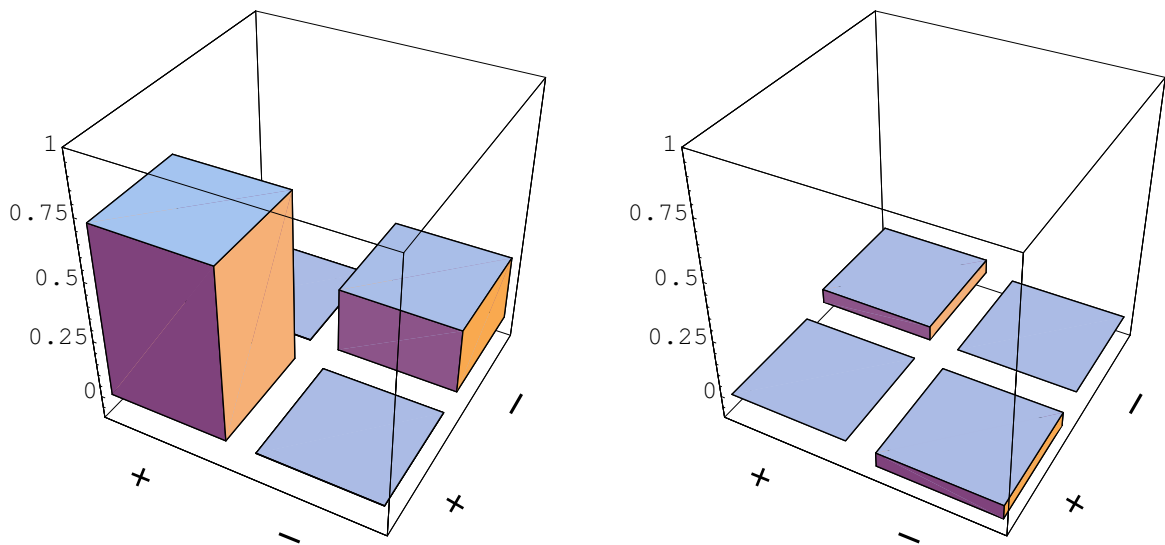


Figure 4.30: Real (left) and imaginary (right) part of the density matrix of clone 1 in the 45° -basis

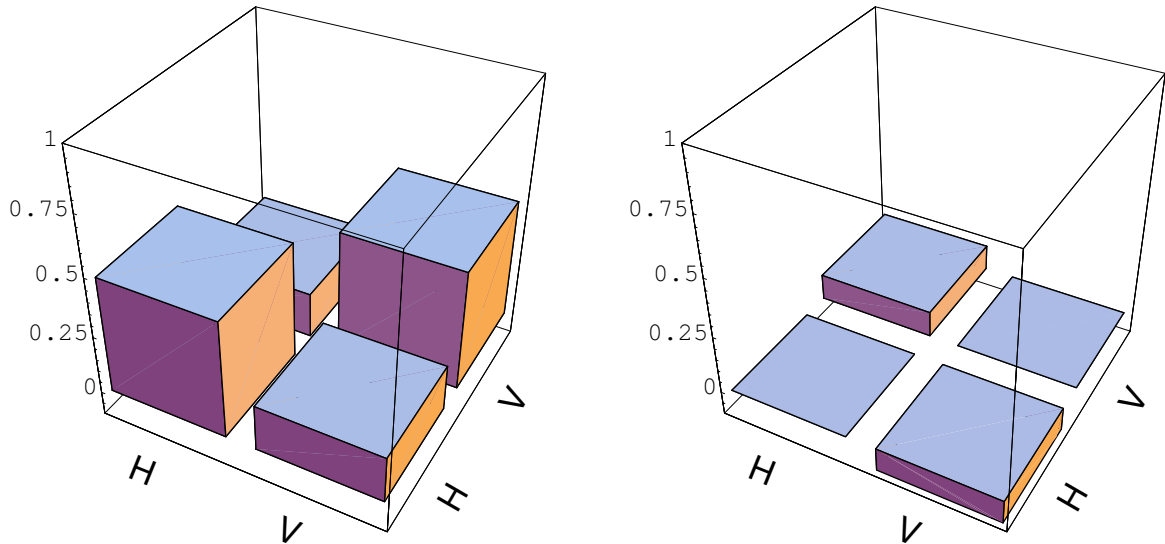


Figure 4.31: Real (left) and imaginary (right) part of the density matrix of clone 2 in the HV-basis

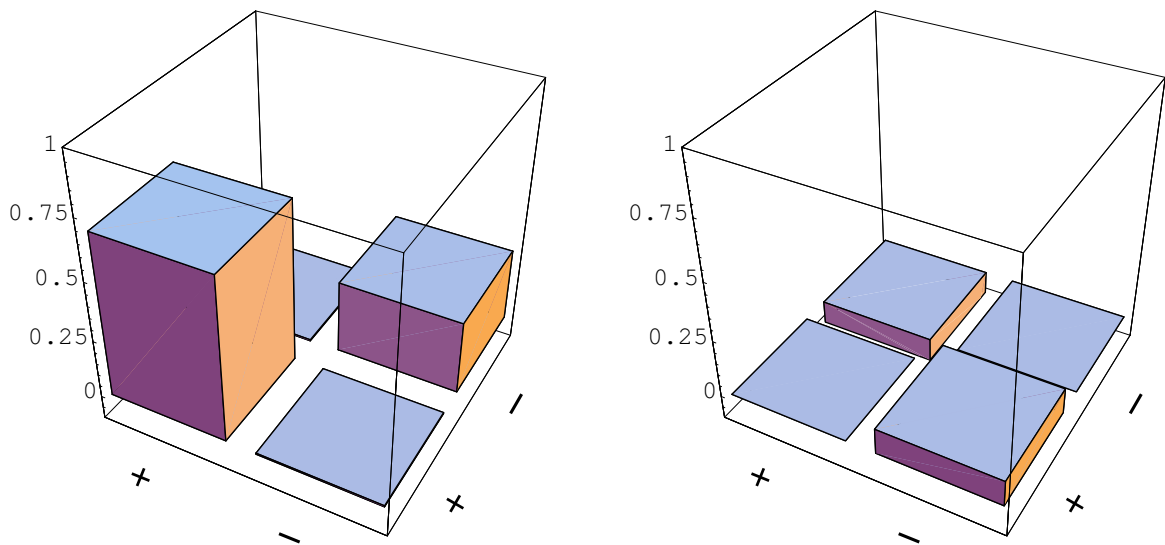


Figure 4.32: Real (left) and imaginary (right) part of the density matrix of clone 2 in the 45°-basis

5 Summary

Quantum telecloning of three different polarisation states of photons was performed successfully within the scope of this thesis. For all input states, where we chose the three complementary polarisation directions $|H\rangle$, $|+\rangle$ and $|R\rangle$, a fidelity of the telecloned states to the input states of about 70% could be achieved. This means that we could realise a universal quantum cloning process, in which the cloned states were communicated to two distant receivers simultaneously. It is universal since it shows equal performance for all kinds of input states, and quantum since the fidelities lie above the classical limit of 66.7%, which is the highest fidelity achievable by a measurement on the input state.

For the implementation of the scheme a four-photon polarisation entangled state was used which we could obtain with high visibility from parametric down conversion, and the input state was realised by the polarisation of a strongly attenuated laser beam. The necessary interference between the weak coherent state and one of the down conversion photons was aligned by utilizing a two photon interference effect, the so called Hong Ou Mandel dip [16].

Before the experimental quantum telecloning was started, quantum teleportation of the same kind of input states was performed. This could be realised with the same experimental setup, just by using first order down conversion emissions instead of second order emissions, for which the countrates are much higher. In this way the setup could be optimised for the subsequent long time measurements. The fidelities for the teleportation of the input states $|H\rangle$ and $|V\rangle$ were about 92%, and about 86% for the input states $|+\rangle$ and $|-\rangle$. This assymetry was due to a particular setup of the Bell state analyser which reduced the background contributions for the teleportation of $|H\rangle$ and $|V\rangle$.

Background contributions also posed the main difficulty for the realisation of quantum telecloning. They were expected to constitute about 26% of the overall countrate which means that there was little room left for our goal to exceed the classical limit for the quality of the clones.

After the universality of the process was proven, we chose one input state, namely $|+\rangle$ for which we studied the states of the copies in more detail by measuring their density matrices. The fidelity of the measured states to the output states predicted by theory were about 99%. The same measurement can be extended to a measurement of the two-photon state of both copies. As shown in the theory chapter those two photons should be entangled, and the hope is to verify this entanglement experimentally in the near future.

A Appendix

A.1 Determination of beam splitter parameters

The **transmissivity** $t_{H,V}^2$ and **reflectivity** $r_{H,V}^2$ for horizontal and vertical polarisation of beam splitters have been measured by using the light of a laser diode as input beam and preparing the respective polarisation by means of a polarising beam splitter and a half wave plate, as shown in Fig A.1. The light intensity in both output modes was measured

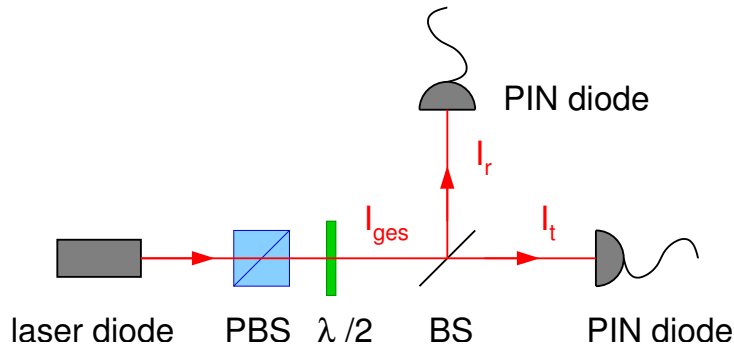


Figure A.1: Setup for the measurement of transmissivity and reflectivity

with PIN diodes. With those values the transmissivities and reflectivities can be calculated like

$$t_H^2 = \frac{I_{t_{H,V}}}{I_{t_{H,V}} + I_{r_{H,V}}} \quad r_H^2 = \frac{I_{r_{H,V}}}{I_{t_{H,V}} + I_{r_{H,V}}}$$

The loss l of the beam splitter can be determined by additionally measuring the intensity I_{ges} in front of the beam splitter:

$$l = \frac{I_{ges} - (I_t + I_r)}{I_{ges}}$$

For a determination of the **phase shift** introduced between horizontal and vertical polarisation components, for example in the reflected beam, the setup shown in Fig. A.2 has been used. The input beam was polarised at $+45^\circ$ and the output beam was analysed in

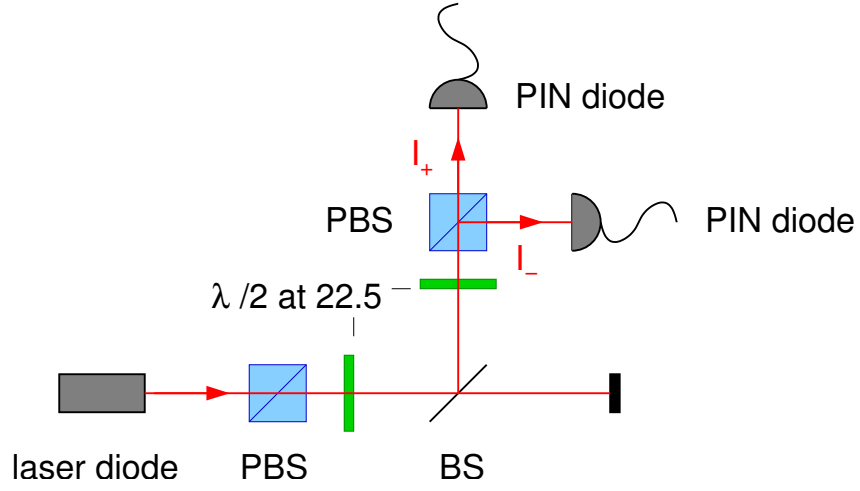


Figure A.2: Setup for the measurement of the phase shift in the reflected beam the 45° -basis. The transformation of the beam splitter in case of a phase shift $\Delta\phi$ is

$$|+\rangle = \frac{1}{\sqrt{2}}(|H\rangle + |V\rangle) \rightarrow \frac{1}{\sqrt{2}}(r_H|H\rangle + r_V e^{i\Delta\phi}|V\rangle) + \text{transmitted part}$$

A projection of this state onto the 45° -basis leads to the following relation

$$\frac{I_+}{I_+ + I_-} = \frac{(r_H^2 + r_V^2 + 2r_H r_V \cos \Delta\phi)}{2(r_H^2 + r_V^2)},$$

with which the absolute value of the phase shift can be calculated.

A.2 Representations of photon states

In this thesis two different representations of multi photon states have been used:

- If all photons occupy different modes, which means that they are distinguishable, just the polarisation and spatial modes of the single photons are indicated, for example

$$|HVVH\rangle_{abcd} = |H\rangle_a |V\rangle_b |H\rangle_c |V\rangle_d$$

means that the photon in mode a is horizontally polarised, etc.

- If there can be more than one photon in a single mode, the photon number representation is used, where the occupation numbers of the different modes are given, for example

$$|2H_a, 1V_b\rangle$$

means two photons with horizontal polarisation in mode a and one photon with vertical polarisation in mode b . The above state written as photon number state would give

$$|HVVH\rangle_{abcd} = |1H_a, 1V_b, 1H_c, 1V_d\rangle.$$

In some cases, where all photons have the same polarisation, the letters indicating the polarisation have been omitted, like

$$|0\rangle_a |2\rangle_b.$$

Those photon number states are also called Fock states.

Bibliography

- [1] M. Muraao, D. Jonathan, M. B. Plenio, and V. Vedral, *Quantum telecloning and multiparticle entanglement* Phys. Rev. A **59**, 156 (1999).
- [2] N. Gisin and S. Massar, *Optimal Quantum Cloning Machines* Phys. Rev. Lett. **79**, 2153 (1997).
- [3] Charles H. Bennett, Gilles Brassard, Claude Crépeau, Richard Josza, Asher Peres, and William K. Wootters, *Teleporting an Unknown Quantum State via Dual Classical and Einstein-Podolski-Rosen Channels*, Phys. Rev. Lett. **70**, 1895 (1993).
- [4] Dik Bouwmeester, Jian-Wei Pan, Klaus Mattle, Manfred Eibl, Harald Weinfurter and Anton Zeilinger, *Experimental quantum teleportation*, Nature **390**, 575 (1997).
- [5] Dagmar Bruß, Artur Ekert, and Chiara Macchiavello, *Optimal Universal Quantum Cloning and State Estimation*, Phys. Rev. Lett. **81**, 2598 (1998).
- [6] Dagmar Bruß and Chiara Macchiavello, *On the entanglement structure in quantum cloning*, quant-ph/0212059.
- [7] Paul G. Kwiat, Klaus Mattle, Harald Weinfurter, and Anton Zeilinger, *New High-Intensity Source of Polarisation-Entangled Photon Pairs*, Phys. Rev. Lett. **75**, 4337 (1995).
- [8] Harald Weinfurter and Marek Żukowski, *Four-photon entanglement from down-conversion*, Phys. Rev. A **64**, 010102-1 (2001).
- [9] S. Gaertner, M. Bourennane, M. Eibl, C. Kurtsiefer, H. Weinfurter, *High-fidelity source of four-photon entanglement*, Appl. Phys. B **77**, 803 (2003).
- [10] W. K. Wootters and W. H. Zurek, *A single quantum cannot be cloned*, Nature **299**, 902 (1982).
- [11] V. Bužek and M. Hillery, *Quantum copying: Beyond the no-cloning theorem*, Phys. Rev. A **54**, 1844 (1996).
- [12] V. Bužek and M. Hillery, *Universal Optimal Cloning of Qubits and Quantum Registers*, in *QCQC'98, LNCS 1509* edited by C. P. Williams, Springer-Verlag Berlin Heidelberg, 235 (1999).

BIBLIOGRAPHY

- [13] Charles H. Bennett, Stephen J. Wiesner, *Communication via One- and Two-Particle Operators on Einstein-Podolski-Rosen States*, Phys. Rev. Lett. **69**, 2881 (1992).
- [14] Klaus Mattle, Harald Weinfurter, Paul G. Kwiat, and Anton Zeilinger, *Dense Coding in Experimental Quantum Communication*, Phys. Rev. Lett. **76**, 4656 (1996).
- [15] C. H. Bennett, G. Brassard and A. K. Ekert, *Quantum Cryptography*, Sci. Am. **267**, 50 (1992).
- [16] C. K. Hong, Z. Y. Ou, and L. Mandel, *Measurement of Subpicosecond Time Intervals between Two Photons by Interference* Phys. Rev. Lett. **59**, 2044 (1987).
- [17] J. G. Rarity and P. R. Tapster, *Interference Between a Single Photon and a Superposition of Coherent States in Quantum Interferometry*, edited by F. De Martini, G. Denardo, and Y. Shih (VCH, Weinheim), 211 (1996).
- [18] S. Massar and S. Popescu, *Optimal Extraction of Information from Finite Quantum Ensembles*, Phys. Rev. Lett. **74**, 1259 (1995).
- [19] Asher Peres, *Separability Criterion for Density Matrices*, Phys. Rev. Lett. **77**, 1413 (1996).
- [20] M. Horodecki, P. Horodecki, R. Horodecki, *Separability of mixed states: necessary and sufficient conditions*, Phys. Lett. A **233**, 1 (1996).
- [21] H. Weinfurter, *Experimental Bell-State Analysis* Europhys. Lett. **25**, 559 (1994).
- [22] P. G. Kwiat, H. Weinfurter, *Embedded Bell-state analysis*, Phys. Rev. A **58**, 2623 (1998).
- [23] Jian-wei Pan and Anton Zeilinger, *Greenberger-Horne-Zeilinger-state analyser*, Phys. Rev. A **57**, 2208 (1998).
- [24] S. Gaertner, C. Kurtsiefer, and H. Weinfurter, *A fast and simple multi-channel photon coincidence unit for quantum communication*, to be published.
- [25] David S. Klinger, James W. Lewis, Cora Einterz Randall, *Polarised Light in Optics and Spectroscopy*, Academic Press (1990).
- [26] Jean-Claude M. Diels, Joel J. Fontaine, Ian C. McMichael, and Francesco Simoni, *Control and measurement of ultrashort pulse shapes (in amplitude and phase) with femtosecond accuracy*, Applied Optics **24**, 1270 (1985).
- [27] Axel Kasper, *Erzeugung und Charakterisierung ultrakurzer Lichtpulse aus Ti:Sa Laser-Oszillatoren*, Dissertation Technische Universität München (1997).
- [28] N. Kiesel *Experimental Analysis of a Three-Photon Entangled State*, Diplomarbeit LMU München (2002).

- [29] Danniell F. V. James, Paul G. Kwiat, William J. Munro, and Andrew G. White, *Measurement of qubits*, Phys. Rev. A **64**, 052312 (2001).
- [30] S. Gaertner, M. Bourennane, C. Kurtsiefer, and H. Weinfurter, *Experimental demonstration of four party quantum secret sharing*, to be published.
- [31] A. Lamas-Linares, J. C. Howell and D. Bouwmeester, *Stimulated emission of polarisation-entangled photons*, Nature **412**, 887 (2001).
- [32] Antia Lamas-Linares, Christoph Simon, John C. Howell, Dik Bouwmeester, *Experimental Quantum Cloning of Single Photons*, Science **296**, 712 (2002).
- [33] S. Gaertner, M. Bourennane, C. Kurtsiefer, H. Weinfurter, *Multiphoton entanglement from parametric down conversion*, to be published.
- [34] Thomas Jennewein, *Synchrone Erfassung von Photodetectionen an entfernten Orten*, Diplomarbeit Universität Innsbruck (1997).
- [35] Harald Weinfurter, *Quantum communication with entangled photons*, Advances in atomic, molecular, and optical physics **42**, 489 (2000).
- [36] Charles Bennett and David P. DiVincenzo, *Quantum information and computation*, Nature **404**, 247 (2000).

Acknowledgements

There are some people whom I would like to specially thank at this occasion.

Harald Weinfurter for giving me the possibility of performing such an exciting experiment, and for offering some helpful advices and discussions. He also gave me the opportunity to attend conferences where I could gain some insight into recent fields of research.

Christian Kurtsiefer for his permanent support and some useful hints which helped to safe days of work. His leaving to Singapur was a real loss.

Many thanks to Sascha Gaertner for introducing me to the lab work, guiding me through the experiment, supporting me whenever needed and, most important, motivating and inspiring me, and helping me not to get frustrated sometimes. With him even hard work could be real fun.

Finally I want to thank my parents for supporting me in all the years of my studies.

Erklärung

Hiermit erkläre ich, dass ich die vorliegende Arbeit selbständig und unter ausschließlicher Verwendung der angegebenen Quellen und Hilfsmittel verfasst habe.

Julia Lau

München, den 16. Februar 2002